Final Report:
"Synthesis and Characterization of Mixed-Conducting Corrosion Resistant Oxide Supports"

PI: Vijay Ramani (Illinois Institute of Technology, IIT); co-PI: Jai Prakash (IIT); subcontractor: Nissan Technical Center, North America (NTCNA), Farmington Hills, MI, USA

Contract Number: DE-EE0000461
Project Start Date: Sep 2010
Project End Date: Jan 2015

Acknowledgment: "This material is based upon work supported by the Department of Energy under Award Number DE-EE0000461."

Index:

Introduction

While Pt supported on carbon is the most commonly used electrocatalyst for PEFCs, the carbon has several limitations as catalyst support: the durability at high temperatures and during the excursions to high electrode potentials that arise during start-up and shut-down sequences and during fuel starvation. The issue of carbon corrosion is a major technical barrier for the development of viable PEMFC commercial applications. Carbon corrosion facilitates the agglomeration of Pt particles and dissolution of Pt from the support, which leads to a loss in the ECSA of the electrode (Landsman and Luczak, 2003). To address this issue, the development of non-carbon mixed-conducting catalyst support materials is explored. Desirable properties of these alternative materials include (i) high surface area; (ii) high electrical conductivity; and (iii) high electrochemical stability. In addition, it is hypothesized that fuel cell performance can be enhanced by utilizing non-carbon catalyst supports that conduct protons on their surface. The addition of sulfonic acid functionalities on the support surface should permit lowering the ionomer content in the electrode, thereby enhancing gas transport to the catalyst site without compromising on the efficacy of ion transport.

1. RuO_2-SiO_2 Catalyst Support

Accomplishments (Lo and Ramani, 2012)

- Demonstrated that the synthesized RuO_2-SiO_2 catalyst supports possess the following properties: a) high BET surface areas ($260 m^2/g$), b) excellent electrical conductivity (up to 24 S/cm), and c) improved electrochemical stability. Start-stop stability tests were performed by cycling electrode potential between 0 V to 1.8 V for 1000 cycles. The results showed no loss in surface area for the RuO_2-SiO_2 catalyst supports, while a 44% drop in surface area was observed in carbon supports tested as a baseline.
- Synthesized functionalized silica supports with several levels of sulfonic acid functionalization. These materials have demonstrated varying degrees of proton conductivity and electrochemical stability.
- Demonstrated fuel cell performance with a platinum catalyst supported on non-carbon catalyst supports synthesized in this study – Pt/RuO_2-SiO_2.

1.1.Approach

To achieve the first of two objectives discussed above, two approaches have been employed. The first approach involves the development of a core–shell-like RuO_2-SiO_2 structure that serves as the catalyst support. High surface area silica functionalized with sulfonic acid groups (HSO_3-) was used as core matrix. This was further functionalized with a shell layer of RuO_2 to introduce electronic conductivity; the final material was calcined at temperatures ranging from 100 – 450°C. The electrochemical stability of RuO_2-SiO_2, Pt/RuO_2-SiO_2, and HSO_3-SiO_2 were measured and compared with that of commercial Pt/C and XC-72R carbon. The electrical and proton conductivities and BET surface areas of materials prepared with different extents of functionalization were also measured.

The second approach involved the synthesis of sulfonic acid functionalized silica with a bimodal pore-structure. The intent of this approach was for RuO_2 to be selectively impregnated in the mesopores of the bimodal structure, while leaving the macropores free for reactant and product transport.

1.2. Synthesis of Ruthenium Oxide-Silica Composite Supports

High surface area SiO_2 was synthesized as follows - Pluronic 123 (18.0 g) was dissolved under stirring in DI water (561 g) and concentrated HCl (99.5 g) at room temperature. Tetraethoxyorthosilane (TEOS, 39.8 g) was added to the solution and stirred for 5 min, followed by stirring at 35 °C for 20 h. The mixture was aged at 80 °C for 24 h to swell the pores. The mixture was decanted to remove most of the solution, and the white solid was filtered and dried at 60 °C for 24 h. The white powder was calcined to remove the polymer template using the following temperature profile: (1) heating to 200 °C at 1 °C /min, (2) holding at 200 °C for 1 h, (3) heating to 550 ◦C at 1 °C /min, (4) holding at 550 °C for 6 h, and (5) cooling to 200 °C at 1 °C /min. This yield SBA-15 silica. RuO_2/ SiO_2 composites were prepared by depositing $RuO_2 \cdot x$H2O on the resultant silica support in an alkaline medium. The SBA-15 was immersed in an aqueous solution containing 0.1 M $RuCl_3 \cdot nH_2O$. Then 0.1 M KOH(aq) was dropped into the mixture under stirring until the pH of the solution reached twelve. The black powder was filtered out and washed repeatedly with distilled water. The solid was dried at 100 °C and calcined at 450 °C. Different composites with RuO_2 mole percent of 9.09, 20, 24.8, 29.6, 33.3, 50, and 60 were synthesized by using this method.

1.3. Characterization of Ruthenium Oxide Functionalized Silica Additives

The key structural attribute studied was the surface area of the resultant support materials, estimated from BET studies. The key transport property studied was the electronic conductivity of the supports, as estimated by a 2-point pellet conductivity probe. The results obtained for the various compositions synthesized are tabulated below. Clearly, the new method adopted in this study permit the synthesis of silica- ruthenium oxide composites with surface areas that are an order of magnitude higher than those obtained in preliminary experiments to provide proof of concept. The materials calcined at 450 °C show higher electrical conductivity, which may be attributed to improved crystal structure through calcination. Improvement in crystallization will be further confirmed by XRD.

Table 1. Properties of ruthenium oxide-silica composite supports synthesized in this project

RuO_2 mole percent	0	9.09	20	24.8	29.6	33.3	50	60
Electrical conductivity (mS/cm)	0.001	7.74±0.15	73.5±4.3	256±23.5	695±10.2	2151±61, 3372±96[a]	10697±261 24223±1238[a]	20254±255
BET surface area (m^2/g)	1100	470				460, 420[a]	260, 310[a]	220

[a]: samples were calcined at 450 °C

As shown in **Figure 1**, increase in conductivity varies with RuO_2 mole percent. The increase in conductivity with RuO_2 mole percent below 40% is greater than that with RuO_2 mole percent above 40%. The difference in slopes below and above around 40 mol% RuO_2 is attributed to the amount of particle contact needed for creating optimal pathways to conduct electrons. While increase in RuO_2 particles under 40mol% creates substantially more pathways to conduct electrons, additional RuO_2 particles beyond 40 mol% do not have as much effect because available pathways with direct contact between particles have been created. This hypothesis will be further confirmed by TEM.

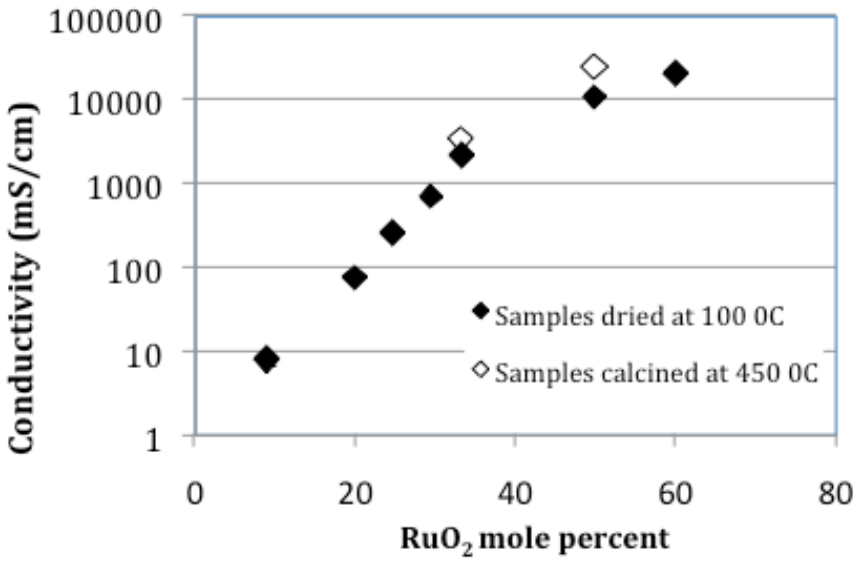

Figure 1. Conductivity of ruthenium oxide-silica composites as a function of the RuO_2 mol content.

Equally promising is the fact that the electronic conductivity of the sample with the 33% RuO_2 loading is still a highly respectable 3 S/cm (silica on its own has a conductivity of 10^{-6} S/cm). These results suggest that the silica-ruthenium oxide system is indeed a viable high surface area catalyst support. Given that the BET surface area is drastically lowered as the amount of RuO_2 in the sample is increased, further research in this area will focus on lowering the RuO_2 content (thereby further increasing surface area) while maintaining or enhancing the electronic conductivity by tuning the distribution of RuO_2 in the silica matrix. To this end, work has been initiated in the synthesis of silica materials with a bimodal pore-structure, wherein the ruthenium oxide can be selectively impregnated in the mesopores, leaving the macropores free for reactant and product transport. The acquisition of the supercritical drier will greatly aid work in this direction by facilitating the formation of high surface area silica with a bimodal pore-structure and further details on this approach will be provided in the following quarterly report.

1.4. Electrochemical Stability of Ruthenium Oxide Functionalized Silica Additives

Stability of the ruthenium oxide functionalized silica supports were characterized by performing potential cycling tests on the ruthenium oxide - silica composite supports coated on a glassy carbon (GC) disk electrodes in N_2 saturated 0.1M $HClO_4$ solution using

a rotating disk electrode (RDE) setup. Catalyst support ink was prepared by adding 3.4 mg of the ruthenium oxide-silica support to a compensatory amount of 5 wt% aqueous Nafion® solution and 0.4 mL of ethanol and the mixture was homogenized by thoroughly mixing over a stir-plate for at least 12 hours. 5 µL of the ink was then applied onto the GC disk using calibrated micropipette and dried under ambient conditions. The final catalyst support loading on GC disk was controlled approximately to 200 µg/cm^2 for all stability experiments. In the RDE setup, a saturated calomel electrode was used as reference electrode and Pt foil was used as counter electrode. The supports were cycled between 0 to 1.8 V vs. RHE at a scan rate of 1 V/s for upto 1000 cycles and cyclic voltammograms were recorded at periodic intervals at a scan rate of 10 mV/s. The CVs were analyzed to assess the double-layer charge of the supports. This metric was employed as a preliminary estimate of support surface area and stability. The stability of the ruthenium oxide- silica composites, pure RuO_2, sulfonic acid functionalized silica and Vulcan XC-72R carbon (baseline) are all shown in **Figure 2.**

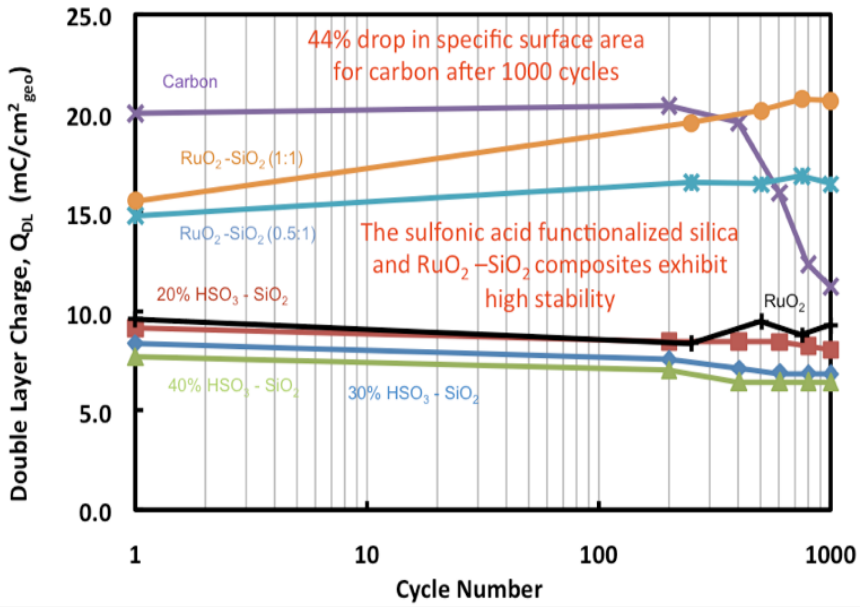

Figure 2. The stability of the ruthenium oxide functionalized silica supports. The supports were cycled between 0 to 1.2 V vs. RHE at a scan rate of 1 V/s for up to 10,000 cycles and intermediate cyclic voltammograms were recorded at 10 mV/s to determine the double layer capacity.

The Q_{DL} was estimated by calculating the charge associated with the double-layer region, where no faradaic reactions occur, from the CVs recorded at 10 mV/s. Both the ruthenium oxide-silica composites showed similar Q_{DL} to that of carbon but exhibited very high stability for up to 1000 cycles in contrast to carbon, which showed a 44% drop in Q_{DL} after 1000 cycles due to carbon oxidation and concomitant loss in surface area. Pure RuO_2 and sulfonic acid functionalized silica showed stable but much lesser double-layer surface area compared to carbon.

1.5. Platinum Deposition on Ruthenium Oxide-Silica Composites

25.2 mg of chloroplatinic acid ($H_2PtCl_6.6H_2O$) was dissolved in 100 mL of de-ionized water in a 500 mL conical flask and the solution was mixed and heated to 80°C on a heated stir-plate for 2 hours. After 2 hours of stirring under heat, 40 mg of catalyst support {SiO_2 or RuO_2-SiO_2 (0.5:1) or RuO_2-SiO_2 (1:1)}was added to the hot solution under stirring and once the support particles are well dispersed in the solution, fresh aqueous sodium borohydride ($NaBH_4$) solution was added slowly dropwise. When added to water, since 1 mole of $NaBH_4$ solution liberates 4 mole of H_2, $NaBH_4$ solution was added at 2 : 1 molar ratio of $NaBH_4$ to the desired amount of Pt.

The high amount of H_2 liberated during $NaBH_4$ addition enabled the reduction of Pt from the solution phase to the metallic phase and the reduced Pt is deposited on the catalyst supports. As the deposition of Pt on the supports grew, the Pt-support particles sedimented to the bottom of the flask leaving a clear solution consisting of $NaBO_2$ and NaCl dissolved in water. The settled particles were then filtered out using vaccum filtration on 0.1 μm cellulose filter. The filtered products were washed with de-ionized water 4 times and the resultant product was dried under vaccum at 80°C to remove the moisture from the prepared Pt-support particles. Platinum precursor and support quantities were adjusted to obtain a 20 wt% Pt deposition on ruthenium oxide-silica supports.

1.6. Electrochemical Stability of 20% Pt on Ruthenium Oxide Functionalized Silica Additives

The stability of the 20% Pt on ruthenium oxide functionalized silica supports were characterized by potential cycling of the catalyst coated glassy carbon (GC) disk electrodes in N_2 saturated 0.1M $HClO_4$ solution using an RDE. Catalyst support ink was prepared by adding 4.3 mg of 20% Pt on ruthenium oxide-silica support to a compensatory amount of 5 wt% aqueous Nafion solution and 0.4 mL of ethanol and the mixture was homogenized by thoroughly mixing over a stir-plate for at least 12 hours. 5 μL of the ink was then applied onto the GC disk using calibrated micropipette and dried in ambient conditions. The final catalyst loading on GC disk was controlled approximately to 50 $\mu g/cm^2$ of Pt and 200 $\mu g/cm^2$ of ruthenium oxide-silica support for all stability experiments. For 57% Pt/C (TANAKA KK; baseline catalyst), the Pt loading was maintained at 147 $\mu g/cm^2$. In the RDE setup, saturated calomel electrode was used as the reference electrode and Pt foil was used as the counter electrode. The supports were cycled between 0 to 1.2 V vs. RHE at a scan rate of 1 V/s for up to 10,000 cycles and intermediate cyclic voltammograms were recorded at 10 mV/s to assess the electrochemical active surface area (ECSA) of the Pt.

The ECSA was calculated from the hydrogen desorption region of the cyclic voltammogram recorded at 10 mV/s. ECSA is calculated from the difference between the total charge involved in the hydrogen desorption and the double-layer charge using the specific H_{upd} charge of 210 $\mu C/cm^2$ on Pt surface. The calculated ECSA values for 20% Pt deposited on Silica (SBA-15), ruthenium oxide- silica composite, ETEK 20% Pt/C and

TANAKA 57% Pt/C are show in the Figure. Ruthenium oxide-silica composites exhibited consistently higher ECSA (> 100 m^2/g_{Pt}), similar to the levels of ETEK Pt/C (115 m^2/g_{Pt}), and the 20% Pt deposited on ruthenium oxide-silica composites were found to be highly stable for upto 10,000 cycles. 20% Pt/SiO_2 and 57% Pt/C showed deterioration of ECSA under this potential cycling test.

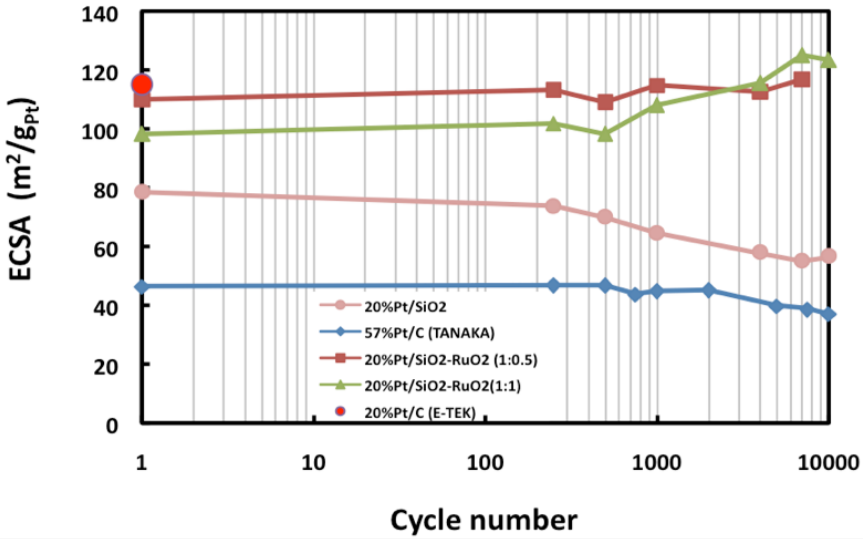

Figure 3. The stability of the 20% Pt on ruthenium oxide functionalized silica supports. The supports were cycled between 0 to 1.2 V vs. RHE at a scan rate of 1 V/s for up to 10,000 cycles and intermediate cyclic voltammograms were recorded at 10 mV/s to determine the electrochemical active surface area (ECSA) of the Pt.

1.7. Fuel Cell Polarization Curves for RuO_2-SiO_2

Preliminary fuel cell performance with RuO_2-SiO_2 (1:1 mole ratio) as the non-carbon support catalyst was obtained. The figure below shows the polarization curves of a PEFC MEA employing 40% Pt/RuO_2-SiO_2 at the anode and the cathode. Measurements were conducted at 80 °C with 75% relative humidity. Reactant flow rates were set at twice the stoichiometric requirement for both H_2 and O_2/air. Pt loading was controlled at 0.4 mg/cm^2 at the cathode and 0.2 mg/cm^2 at the anode. The current density at 0.6 V was 750 mA/cm^2 and the maximum power density obtained was 570 mW/cm^2 under H_2/O_2.

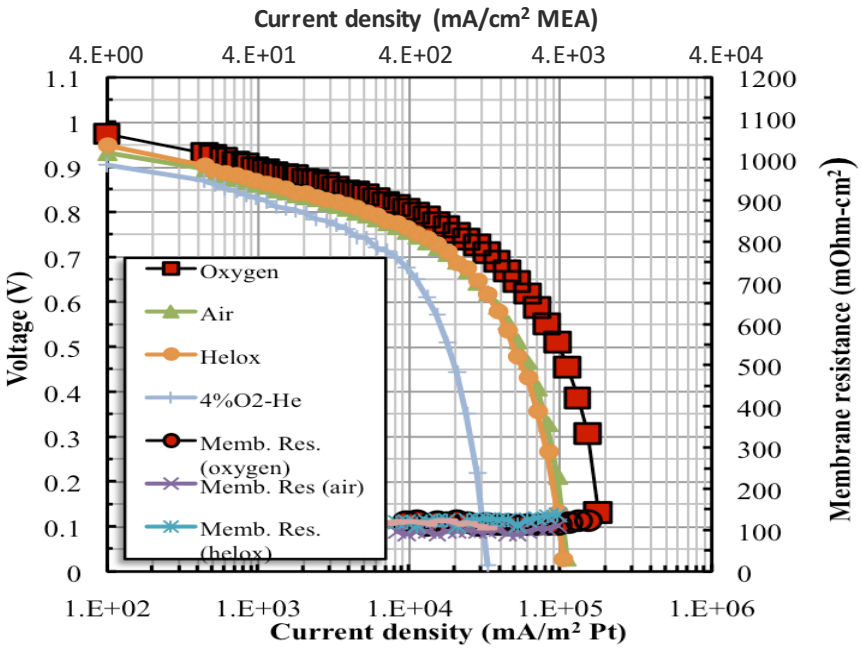

Figure 4. Fuel cell polarization curves for RuO_2-SiO_2 (1:1 mole ratio). Experiments were done at 80 °C with 75% relative humidity. Reactant flow rates were twice the stoichiometric requirements for both H_2 and O_2/air. Pt loading was 0.4 mg/cm^2 at the cathode and 0.2 mg/cm^2 at the anode. The ECSA for 20% Pt deposited on RuO_2-SiO_2 (1:1 mole ratio) was 100 m^2/g_{Pt}. The ECSA for ETEK Pt/C was 115 m^2/g_{Pt}.

2. Silica Functionalized with Sulfonic Acid

2.1. Synthesis of Sulfonic Acid Functionalized Silica Supports

4g of Pluronic 123 was dissolved under stirring in 125 g of 1.9 M HCl at room temperature. The solution was heated to 40°C, and TEOS was added. The mixture was stirred for 45 min for pre-hydrolysis prior to the addition of MPTMS (mercaptopropyltrimethoxysilane) and an aqueous solution of H_2O_2 (30% wt) to the mix. The purpose of the MPTMS was to provide mercapton (-SH) functionality within the resultant silica gel, while the hydrogen peroxide was added to oxidize these mercapton groups to sulfonic acid groups during the gelation process. The molar composition of the mixture for 4 g of copolymer was: 0.041(1-x) TEOS : 0.041x MPTMS: 0.0369 H_2O_2 : 0.24 HCl : 6.67 H_2O; where x was chosen in the first instance to be 0.2, 0.3, and 0.4. The solution obtained was stirred for 20 h at 40 °C and was aged at 100 °C for 24 h under static conditions. The solid product thus obtained was recovered by filtration and air-dried at 60 °C overnight. The polymer template was removed from this material by treatment in ethanol (with reflux) for 24 h. 100% sulfonic acid functionalized silica was synthesized with the following method. 2.7 mL of deionized water, 20 mL of ethanol, 0.2 mL of 37% hydrochloric acid, and 23 mL of mercaptopropyl triethoxysilane (MPTEOS) were mixed together with a nitrogen blanket. The mixture was refluxed for 36 hours at 60 °C. A

viscous liquid was obtained after the removal of the solvent by a rotary evaporator. The liquid was washed with methanol to remove unreacted MPTEOS. Then 20 ml of H_2O_2 (30% wt) was added to oxidize these mercapto groups to sulfonic acid.

2.1.1. Synthesis of Sulfonated Polyhedral Oligosilsesquioxane (SPOSS)

Octaphenyl-POSS (5 g, 4.8 mmol) was added to chlorosulfonic acid (18 mL, 0.27 mol) and was stirred overnight at room temperature. Unreacted chlorosulfonic acid was removed with rotary evaporator and then DI water was added to dissolve the crude product. The volume was reduced to 10 mL under reduced pressure. The particles were washed three times with anhydrous tetrahydrofuran and dried at 60 °C overnight.

2.1.2. Synthesis of Silica Aerogels Functionalized with Sulfonic Acid

Functionalized silica aerogels were synthesized by mixing 1-x mmol tetramethyl orthosilicate (TMOS), x mmol mercaptopropyl-trimethoxysilane (MPTMS), 15 mmol methanol, 4 mmol water and 0.075 mmol NH_4OH. Degrees of functionalization (x) of 0, 33, 50 and 67 mol% (MPTMS/ MPTMS+TMOS) were used in this study. After gelation, the gels were aged for at least 48 hours to ensure complete condensation and later kept for 5 hours in 35 wt% H_2O_2 to oxidize the surface thiol groups to sulfonic acid. The gels were then washed 8-12 times with acetone over 3-4 days to completely exchange all the water inside the pores as well to remove the unreacted precursors. The acetone-loaded gels were then introduced into a supercritical dryer (SFT-100, Supercritical Fluid Technologies, Inc.), and the acetone was removed using supercritical CO_2 extraction (45 °C and 4000 psi). Gel shrinkage during the supercritical drying step was minimal.

2.2. Characterization of Sulfonic Acid Functionalized Silica Additives

Ion exchange capacity (IEC) measurements were performed to ascertain the extent of functionalization with sulfonic acid groups. The surface area of the additives was determined by performing BET experiments. Finally, the proton conductivity of the additives was estimated using a two-point pellet conductivity probe under controlled temperature and relative humidity conditions.

The presence of sulfonic acid groups in these samples was confirmed by IEC measurements, which revealed that the samples had an IEC of 1.7-2.1 meq/g. The IEC did not change sunbstantially with extent of functionalization, but was much higher than the near zero IEC obtained for unfunctionalized silica samples. The BET surface areas of the functionalized silica samples are tabulated. The BET surface area decreases as the extent of functionalization is increased. This offers an explanation as to why the measured IEC does not change with extent of functionalization – the corresponding decrease in BET surface area suggests that a smaller fraction of the ion exchange sites are at the surface of the additive.

Table 2. Properties of sulfonic acid functionalized silica additives synthesized in this project.

Sample	BET surface area (m^2/g)
20% SO_3H-SiO_2	650
30% SO_3H-SiO_2	520
40% SO_3H-SiO_2	450

Finally, preliminary proton conductivity measurements were performed at 40, 60, 80 and 90 °C at 100% RH for samples with 30, 40 and 100% extent of functionalization. A maximum proton conductivity of 140 mS/cm was obtained for 100 % functionalized SiO_2 (this is 5-6 orders of magnitude higher than the conductivity of non-functionalized silica, which is on the order of 10^{-6} S/cm), while 30 and 40% functionalized SiO_2 had much lower proton conductivities in the range of 7-25 mS/cm. The results suggest that high functionalization of SiO_2 provides sufficient sulfonic acid groups at the surface, which allows for more efficient proton transfer. However, the 100 % functionalized SiO_2 is not thermally stable and decomposes at around 100 °C. There are two approaches to solving the problem. One apporach is to lower the functionalized ratio to achieve a balance between conductivity and thermal stability. However, this will reduce the conductivity. The other approach is to use a different type of silica that has a higher thermal stability, such as, Polyhedral Oligomeric Silsesquioxanes (POSS).

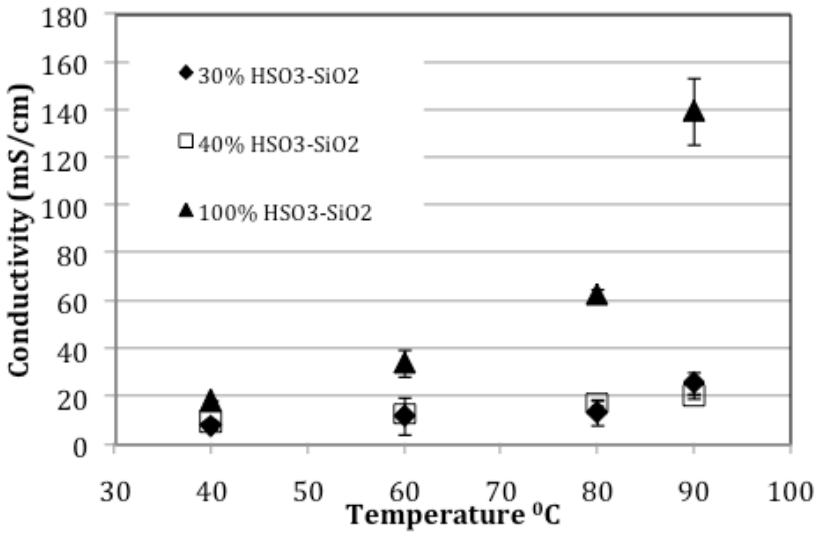

Figure 5. Conductivity of sulfonic acid functionalized silica additives as a function of the temperature.

From the work performed previously, it was found that functionalized silica synthesized with a surfactant-templated sol-gel method was not thermally stable. The experiments were repeated to ensure that the observed instability was not caused by experimental error. The BET surface area of these materials could not be measured because the silica decomposed during the degasing process at 150 °C. Because

functionalized silica synthesized with the surfactant-templated sol-gel method did not seem to be a promising candidate, alternative synthesis approaches were explored. Two alternate variants of sulfonated silica were synthesized this quarter: sulfonated polyhedral oligosilsesquioxane (SPOSS) and functionalized silica aerogel.

The surface morphology was observed by scanning electron microscopy (Figure 6). Ion exchange capacity (IEC) measurements were performed to ascertain the extent of functionalization with sulfonic acid groups. The surface area of the additives was determined by BET results. Finally, the proton conductivity of the additives was estimated using a two-point pellet conductivity probe under controlled temperature and relative humidity conditions.

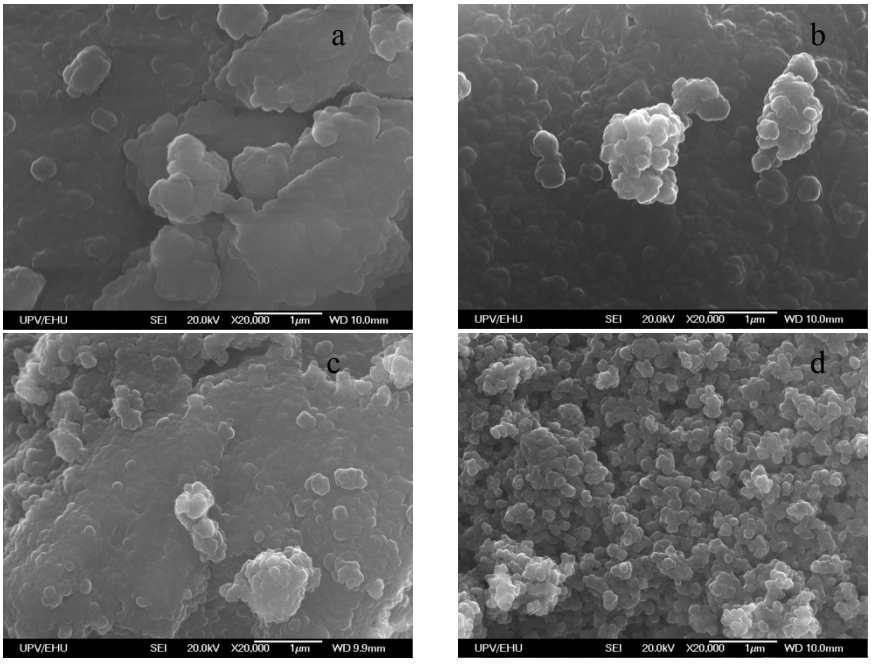

Figure 6. Scanning electron microscopy (SEM) of sulfonic acid functionalized silica additives.

The incorporation of MPTMS induced indirect changes in the sol-gel process. MPTMS basically acted as a co-solvent in the first phase of the reaction when the TMOS was condensing. Therefore, TMOS was more diluted at this stage, resulting in a decrease in the network density, and a larger amount of water and NH_4OH was available for the condensation reactions. These changes in the gelation conditions produced larger nanoparticles and hence decreased the surface area of the gel. The morphological changes in the gels with varying MPTMS contents are shown in the SEM images above (a-d corresponds to increasing functionalization from 0-67%). A tendency towards discrete particle formation instead of gelation was observed when using greater amounts of MPTMS. These changes were also accompanied by decreases in the BET surface area and the pore volume (Table 3).

Table 3. Properties of the functionalized silica aerogels

Functionalization degree, %	Ion exchange capacity, mmol/g	BET surface area, m^2/g	Pore volume, cm^3/g	Average pore diameter, nm
0	0	944±63	2.4	10.1
33	1.4	499±8	1.0	8.4
50	1.7	233±2	0.6	9.6
67	2.1	116±3	0.2	8.3

Although SPOSS exhibited a higher proton conductivity as shown in **Figure 7**, it was also thermally unstable and dissolved in water at higher temperature. The proton conductivity of SPOSS heated at 150 °C for ten minutes decreased to 50 mS/cm at 90 °C and 100%RH.

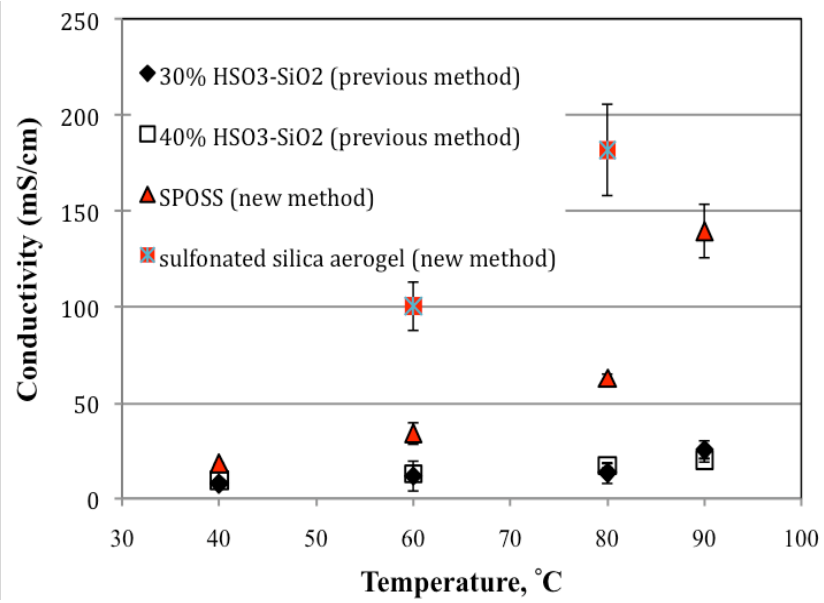

Figure 7. Proton conductivity of SPOSS and sulfonated silica aerogel at 100%RH as a function of the temperature.

Even though the IEC of the functionalized silica aerogels increased from 1.4 to 2.1 mmol/g, little change was observed in the ionic conductivities of the silica with extent of functionalization (33, 50 and 67mol%). The conductivity at each extent of sulfonation was measured three times at four temperatures (60, 80, 100 and 120^{o}C) and four relative humidities (25, 50, 75 and 100%RH). The conductivity variations between the samples with different extents of functionalization were within the measured experimental error at all conditions; the values obtained are shown in **Figure 8**.

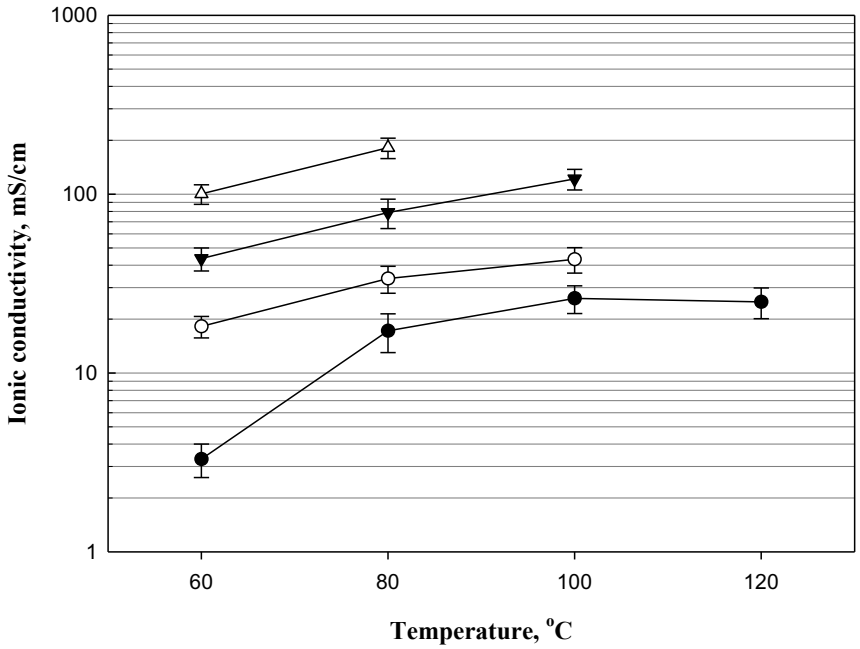

Figure 8. Proton conductivity of sulfonated silica aerogel at (●) 25% relative humidity (RH), (○) 50% RH, (▼) 75% RH and (△) 100% RH as a function of the temperature.

The result may appear to be unexpected at first glance but in fact is interpretable when factors affecting the ionic conductivity were considered. Ionic conduction in these materials was essentially a surface phenomenon and hence was affected by both the surface area and the concentration of charge carriers (sulfonic acid groups) per unit surface; an increase in both would increase ionic conductivity. As the degree of functionalization was increased, so were the IEC and hence the surface concentration of sulfonic acid groups. However, the BET surface area decreased considerably. The increase of IEC and carrier groups was offset by the concomitant decrease of internal surface, leading to a constant value for ionic conductivity.

The functionalized aerogels showed ionic conductivities ranging from 1 to 200 mS/cm. The conductivity increases with both temperature at a fixed relative humidity, as well as with relative humidity at a fixed temperature. These observed values for the conductivity were considerably higher than those reported in previous literature. The improvement could be attributed to the exceptional properties of aerogels, which has higher surface areas and more open pore structure that favored ionic mobility.

The functionalized silica aerogels possess high thermal stability, which is another desirable property. The conductivity of 33 mole% functionalized silica remained the same when annealed at 180 ^{o}C for 15 min.; the conductivity of 33 mol% functionalized silica annealed at 330 ^{o}C for 2 hours was around 60 mS/cm. These aerogels are also being employed as additives for composite membranes for hydrogen-air and direct methanol fuel cells.

2.3. Synthesis of ruthenium oxide/sulfonic acid functionalized silica supports

RuO_2/sulfonic acid functionalized SiO_2 composites were prepared by depositing $RuO_2 \cdot x$H2O on the resultant silica support. The 33 mol% functionalized silica was immersed in an aqueous solution containing 0.1 M $RuCl_3 \cdot nH_2O$. Then 0.1 M KOH(aq) was dropped into the mixture under stirring until the pH of the solution reached 7. The black powder was filtered out and washed repeatedly with distilled water. The solid was dried at 100 °C and calcined at 330 °C for 2 hours. The weight ratio of ruthenium oxide to sulfonic acid functionalized silica was 0.8:1.

2.4. Characterization of Ruthenium Oxide/Sulfonic Acid Functionalized Silica

Protons were conducted mainly on the surface of sulfonic acid functionalized silica. Therefore, the loading of RuO_2 should be low enough to prevent blocking of proton conduction. On the other hand, the low loading of RuO_2 reduces the electrical conductivity of the material. The 0.8:1 weight ratio of ruthenium oxide/sulfonic acid functionalized silica was chosen for the initial trial. The composite material possessed electrical conductivity of 0.36 S/cm and a BET surface area of 130 m^2/g. The IEC of the composite material, 0.57 mole/g, was slightly lower than the theoretical value of 0.61 mol/g. The result suggests that the deposited RuO_2 did not block most of sulfonic acid groups on the surface. Therefore, higher RuO_2 loadings will be employed in future to increase electrical conductivity.

2.5. Electrochemical Stability of Sulfonic Acid Functionalized Silica Additives

Electrochemical stability characterizations were performed in a three-compartment electrochemical cell in 0.1 M $HClO_4$: a glassy carbon disk (0.196 cm^2) was used as the working electrode; a saturated calomel electrode (SCE) was used as the reference; and a Pt foil was used as the counter electrode. Catalyst support ink was prepared by adding 4 mg of silica support to a compensatory amount of 5 wt% aqueous Nafion solution and 0.8 mL of ethanol. The mixture was then homogenized by thoroughly mixing by sonication. 8 μL of the ink was then applied onto the GC disk using calibrated micropipette and dried in ambient conditions. The final catalyst support loading on GC disk was controlled to approximately 38 μg/cm^2 for all stability experimentsThe supports were cycled between 0 to 1.8 V vs. RHE at a rapid scan rate of 1 V/s for up to 1000 cycles. Intermediate cyclic voltammograms were recorded at a rate of 20 mV/s to assess the double-layer charge of the supports. Double-layer charge was obtained by calculating the charge involved in the double-layer region, where no faradaic reaction occurs. **Figure 9** shows the comparison of the stability results of sulfonic acid functionalized silica aerogel (annealed at 330 ^oC for 2 hours), ruthenium oxide- sulfonic acid functionalized silica aerogel composite (annealed at 330 ^oC for 2 hours), and Vulcan XC-72R carbon, along with some prior results for comparison. Annealed sulfonic acid functionalized silica aerogels remained stable for up to 1000 cycles, whereas carbon showed a 44% drop in double-layer surface area after 1000 cycles. The stability of the composite is discussed in a subsequent section.

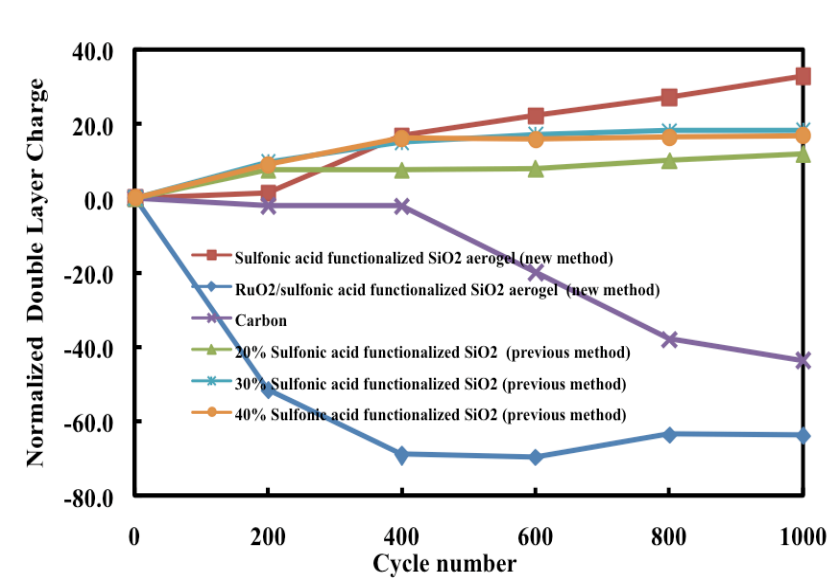

Figure 9. Electrochemical stability of sulfonic acid functionalized silica additives.

3. RuO_2-TiO_2 Catalyst Support

Accomplishments (Lo et al., 2013; Parrondo et al., 2014)

- Demonstrated that the synthesized RuO_2-TiO_2 (TRO) catalyst supports possessed the following properties: a) excellent electrical conductivity (~ 22 S/cm), b) excellent electrochemical stability, and c) comparable fuel cell performance with Pt/C baseline. Start-stop stability tests for stand alone supports and MEAs were performed by potential cycling of the cell between 1 V to 1.5 V vs NHE for 10000 cycles. Tests performed both at IIT and Nissan Technical Center, North America (NTCNA) and have confirmed support durability.
- Tests at NTCNA have confirmed that using the RTO supports synthesized and catalyzed at IIT, the beginning of life performance is exactly equal to end of life performance in an MEA that has been subjected to severe start-stop cycling (1-1.5 V, 10,000 cycles). This is in sharp contrast to baseline Pt/C catalyst that shows significant performance deterioration.

3.1. Synthesis of Titanium Oxide-Ruthenium Oxide Supports (TiO_2-RuO_2)

Core-shell-type TiO_2-RuO_2 catalyst supports were prepared with a simple wet chemical procedure. In a typical synthesis procedure, 1 g commercial TiO_2 (P25) was dispersed in 250 ml DI water and sonicated for 30 minutes. 2.59 g $RuCl_3.xH_2O$ was added into the mixture under stirring for 30 minutes. Then, 0.05 N KOH(aq) was dropped into the mixture under stirring until the pH of the solution reached seven. The black powder was filtered out and washed repeatedly with distilled water. The collected particles were dried at 120°C for 8 hours and were named hydrous TiO_2-RuO_2. The hydrous TiO_2-RuO_2 particles were further calcined at 450°C for 3 hours in air and were named anhydrous TiO_2-RuO_2. The mole ratio of Ru:Ti was 1:1.

3.2. Characterization of Titanium Oxide-Ruthenium Oxide Supports

XRD was used to confirm the presence of ruthenium oxide particles on the support and to obtain a quantitative estimate of their crystallite size. The main diffraction peaks around 26°, 38.5° and 49° arose from diffractions attributed to the TiO_2 (101), (004) and (200) planes, respectively (see **Figure 10**). No peak from RuO_2 was observed for the powder dried at 120°C. As the support was calcined at 450°C, the main diffraction peaks of RuO_2 around 28°, 36° and 55° arose from diffractions at (110), (101) and (211) planes, respectively. The results show that hydrous particles consist of amorphous RuO_2 phases. No signal corresponding to a single metallic phase of Ru was detected. Because the supports were prepared with ambient pressure drying without using any surfactant, the materials in hydrous and anhydrous forms exhibited low and similar BET surface area, 30±3 m^2/g. The electrical conductivities of anhydrous support and hydrous support were 22±4 and 10±3 S/cm, respectively.

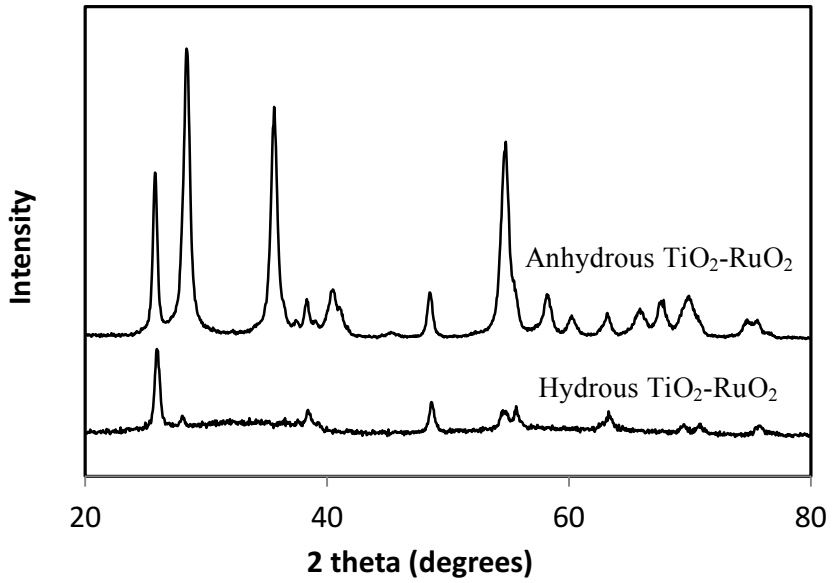

Figure 10. X-ray diffractograms for TiO_2-RuO_2 electrocatalyst supports.

3.3. Synthesis of Platinum Supported on Titanium Oxide-Ruthenium Oxide Catalyst (Pt/TiO_2-RuO_2)

Platinum nanoparticles were synthesized by the chemical reduction of Pt precursor with formic acid. In a typical synthesis, a suspension of 0.54 g TiO_2-RuO_2 support in reaction solution (0.96 g $H_2PtCl_6 \cdot 6H_2O$ and 30 mL HCOOH in 600 mL of water) was sonicated for 30 minutes. All aqueous solutions were prepared with DI water from a Millipore water system. After this initial dispersion, the solution was heated at 80 °C for 2 hours under vigorous stirring. The product was collected by vacuum filtration and washed several times with DI water, and then dried in an oven at 60 °C. Heat treatment was conducted at different temperatures for further use in characterization and electrochemical measurements.

3.4. Characterization of Platinum Supported on Titanium Oxide-Ruthenium Oxide Catalyst (Pt/TiO_2-RuO_2)

Figure 11 shows the XRD patterns of Pt deposited on (a)Pt/anhydrous TiO_2-RuO_2 (b) Pt/anhydrous TiO_2-RuO_2 with heat treatment at 450 °C and (c) Pt/hydrous TiO_2-RuO_2 (see **Figure 11**). It is evident that both catalysts consist of crystalline Pt particles. The main diffraction peaks around 39°, 46° and 68° arose from diffractions at Pt (111), (200) and (220) planes, respectively. The crystallite size was then estimated using the Scherrer equation. The average Pt crystallite sizes for support materials annealed at 120 °C and 450°C are almost identical, 6.2 nm, which indicated that Pt deposition was not affected by support materials. Furthermore, with heat treatment, Pt crystallite size increased from 6.2 nm to 14 nm, indicating the aggregation of Pt particles. Pt also formed an alloy with the support, as revealed by the shift of Pt peak.

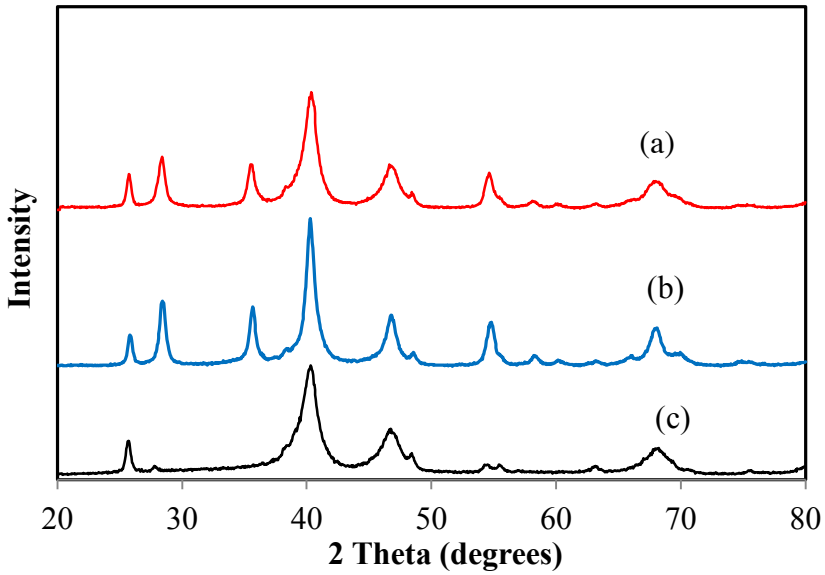

Figure 11. X-ray diffractograms of Pt deposited on (a) Pt/anhydrous hydrous TiO_2-RuO_2 (b) Pt/anhydrous hydrous TiO_2-RuO_2 with heat treatment at 450 °C and (c) Pt/hydrous hydrous TiO_2-RuO_2.

TEM images of Pt/anhydrous TiO_2-RuO_2 catalyst are shown in the figure below (see **Figure 12**). Clearly, Pt nanoparticles were not dispersed uniformly on the support surface. The aggregation of Pt nanoparticles was attributed to the low BET surface area of anhydrous TiO_2-RuO_2 support. The dimensions of the separated Pt nanoparticles were in the range of 3-5 nm. The elemental mapping of Pt/anhydrous TiO_2-RuO_2 catalyst revealed that TiO_2 core was not completely covered by RuO_2 shell and Pt nanopartilces were mainly deposited on the surface of RuO_2.

3.5. Stability Characterization of Titanium Oxide-Ruthenium Oxide Supports (TiO_2-RuO_2)

The degradation of supports can be evaluated by repeated cyclic voltammetry (CV) cycles with the appropriate lower and upper potential limits in an acid solution. Our durability test for the support, which followed the protocol by NTCNA, were conducted by cycling the electrode potential between 1 and 1.5 V versus a reversible hydrogen electrode (RHE) at a scan rate of 500 mV/s in a nitrogen purged 0.1 M $HClO_4$ solution at room temperature. The cyclic voltammograms for Vulcan XC-72 carbon showed a significant increase of double layer capacitance (+220%) and moderate reduction for anhydrous TiO_2-RuO_2 (-4.8%) as the number of cycles increased, where double layer capacitance was calculated by dividing the double layer current at 0.4 V using by the potential scan rate (see **Figure 13**).

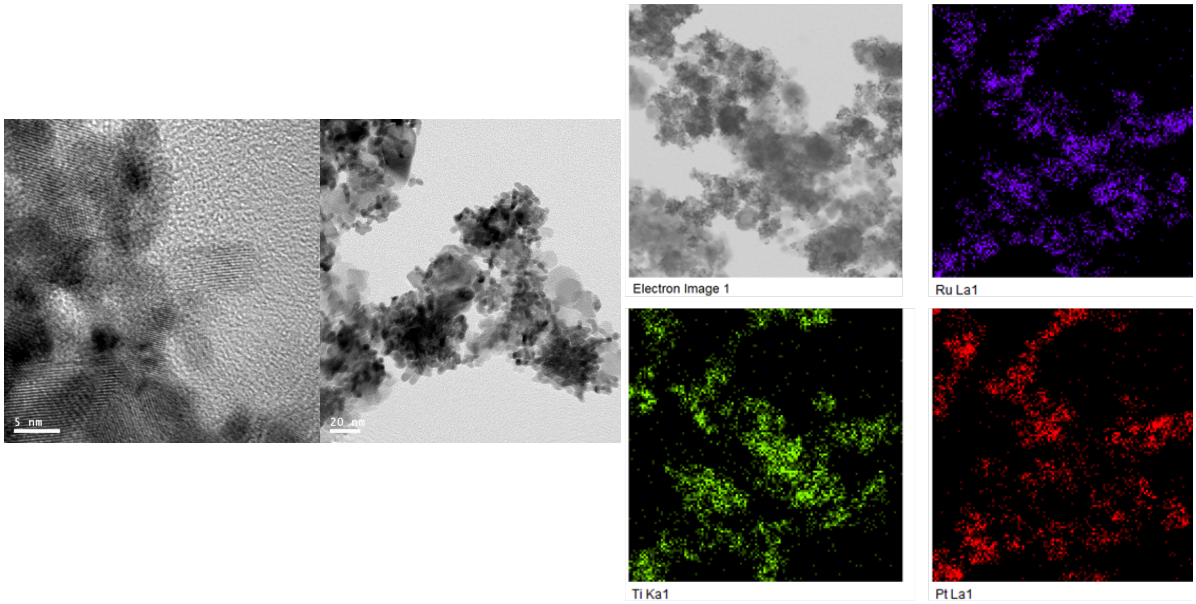

Figure 12. TEM images of Pt/anhydrous TiO_2-RuO_2 catalyst.

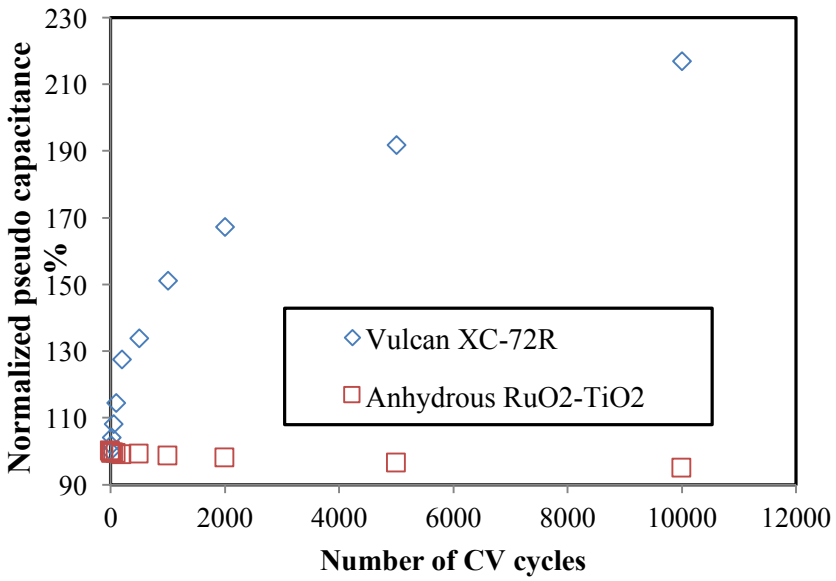

Figure 13. Electrochemical stability (start-stop cycling protocol) of titanium oxide-ruthenium oxide supports (TiO_2-RuO_2).

3.6. Characterization of Platinum Supported on Titanium Oxide-Ruthenium Oxide Catalyst (Pt/TiO_2-RuO_2): ORR Measurements, Electrochemical Stability and Fuel Cell Performance.

The electrochemical stability of the support (TiO_2-RuO_2, TRO) and catalyst (Pt/TRO) were evaluated using accelerated stress test protocols (AST) developed by the Fuel Cell Technical Team of the U.S Drive Partnership in collaboration with the U.S. Department of Energy (Han et al., 2011). The idea behind establishing such protocols was, as it was discussed earlier, to have set of standardized testing methods to evaluate fuel cell performance and durability across laboratories, thereby allowing a proper comparison of the results obtained at different facilities and permitting proper evaluation of technologies/materials resulting from various funded projects. In this study, we used two different protocols that measure **(a)** the stability of the support due to start/shutdown voltage spikes, either stand-alone support or catalysed support, the latter to investigate the impact of platinum catalyst on the support corrosion rate (**start-stop protocol**) (Ohma et at., 2006) and **(b)** Platinum catalyst degradation due to dissolution/Ostwald ripening as a consequence of load cycling - excursions to near the open-circuit potential - during normal fuel cell operation (**load cycling protocol**) (Ralph and Hogarth, 2002; Ohma et al., 2006) These protocols effectively imitate and induce, in an accelerated fashion, the degradation mechanisms that occur during extended normal fuel cell vehicle operation. They were the same protocols employed through all the project to evaluate the stability of all the catalysts and supports.

To evaluate the stability of the support using the start-stop protocol, the working electrode potential was cycled in a triangular waveform between 1.0 V to 1.5 V at a scan rate of 500 mV/s (triangular wave form) for 5,000 cycles. Cyclic voltammograms (CV) were recorded initially (baseline) and after 100, 200, 500, 1000, 2000, and 5000 cycles to characterize the support by estimating the electrode pseudo-capacitance (or, in an equivalent method, the current at 0.4V in the capacitive region of the CV). To evaluate the stability of the platinum catalyst under load cycling, the cathode potential was cycled in a rectangular waveform from 0.95 V (near the open circuit voltage; approaching no-load conditions) to 0.6 V (close to the maximum power; approaching full load conditions) for 10,000 cycles. See Fig 1b. CVs were recorded initially, and after 100, 200, 500, 1000, 2000, 5000 and 10000 cycles. The stability of the catalyst was evaluated from the measured change in ECA and in electrode polarization.

The support and catalyst were examined with both protocols described above. The experiments were performed both *ex-situ* - on supports/catalysts deposited onto a glassy carbon rotating disk electrode (RDE) and *in-situ* - in a fully assembled fuel cell. The experiments were always performed with the working electrode placed in a nitrogen environment to minimize side reactions. Pt/TRO catalyst synthesized in our laboratories was compared against Pt on high surface area carbon (Tanaka 46%; Pt/HSAC).

The durability *ex-situ* experiments were performed in an RDE setup at 60^oC using 0.1M perchloric acid as the electrolyte, a carbon rod counter electrode, and a reversible hydrogen reference electrode. Both CV (at a scan rate of 50 mV/s) and linear polarization

(scan rate of 10 mV/s, various rotation rates) were performed at room temperature for ORR evaluation.

The *in-situ* experiments were performed in a 25cm^2 single fuel cell. MEAs were prepared using a Nafion® 211 membrane, with anode catalyst loading of 0.4 mg/cm^2 Pt/HSAC, and cathode catalyst loading of 0.35 mg/cm^2. The experiments were performed at 80°C, passing hydrogen (0.5 L/min) through the anode (counter and pseudo-reference electrode) side and nitrogen through the cathode/working electrode (0.5L/min). The gases were humidified at either 100% relative humidity (RH) or 40% RH prior to entry into the cell. The 100% RH operating point was chosen to maximize carbon corrosion during the accelerated test (at high voltage, carbon corrosion requires water). The 40% RH condition was chosen as a possible operating point for the fuel cell stack in an automobile. CV and V-I polarization curves were obtained at the beginning and end of the potential cycling tests for each of the MEAs tested. The V-I polarization curves were obtained at 100% and 40% relative humidities, using hydrogen as fuel and air as oxidant.

Initially, several preliminary experiments were performed to ascertain whether the *in-situ* and *ex-situ* approaches yielded similar results. Without a doubt, both methods yielded near identical results in terms of induced loss in ECA upon exposure to said protocols. Subsequently, both catalysts were exposed to the start-stop protocol *ex-situ*, and the impact of this test on the catalyst was studied using CV. The results are shown in **Figure 14**. Pt/TRO did not show any sign of surface modification or instability, as observed for Pt/HSAC, and the H_2 adsorption peak potential did not shift unlike in Pt/HSAC. Both observations indicated the superior stability of the TRO support upon potential cycling. The ratio of ionomer to support (well studied for Pt/C) was then optimized for the Pt/TRO catalyst via an *ex-situ* RDE study. An optimal I/C (ionomer to catalyst ratio) value of 0.58 g/g was obtained (contrast with 0.43 for Pt/HSAC). The ECA, ORR mass and specific activities, number of electrons transferred during the ORR, and the Tafel slopes for the ORR were measured for both catalysts at their optimal I/C ratios. **Figure 16** to **Figure 20** and the accompanying discussion describes the results in more detail. Briefly, the Pt/TRO had lower ECA and mass activities, but a higher specific activity than Pt/HSAC due to the larger platinum particle size (4-6 nm) in Pt/TRO (see **Figure 15**). The number of electrons transferred during the ORR was estimated from a Levich plot to be 3.9 for Pt/HSAC, and 3.2 for Pt/TRO; the Tafel slopes estimated from Koutecky-Levich analysis were 80 and 94, respectively. The ECA, mass activity (i_m) and specific activity (i_s) of Pt/TRO and Pt/HSAC were then estimated for both catalysts upon exposure to the start-stop protocol *ex-situ* (see **Figure 21**). The TRO support showed much better stability than carbon. The loss in ECA, mass activity and specific activity after 5000 start-stop cycles were, respectively, 16%, 14%, and 2% for Pt/TRO. In comparison, Pt/HSAC was much more severely degraded. Its ECA dropped by 40%, mass activity dropped by 55% and specific dropped by 25%. These *ex-situ* studies suggested that TRO was a very stable support and that Pt/TRO was indeed a much more stable electrocatalyst than Pt/HSAC, albeit perhaps less active due to the larger platinum particle size.

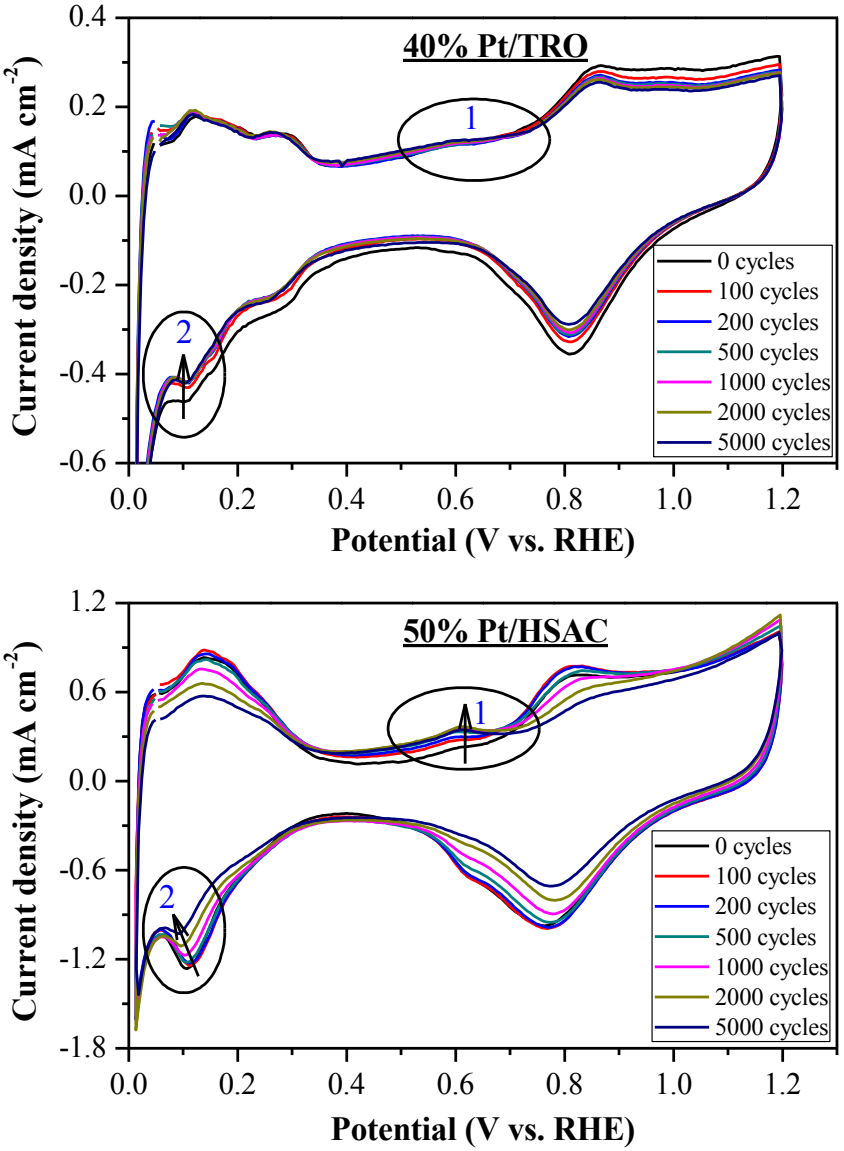

Figure 14. Cyclic voltammograms (scan rate 50mV/s) obtained on 40% Pt/TRO and 50% Pt/HSAC catalysts tested *ex-situ* (RDE) using the start-stop protocol.

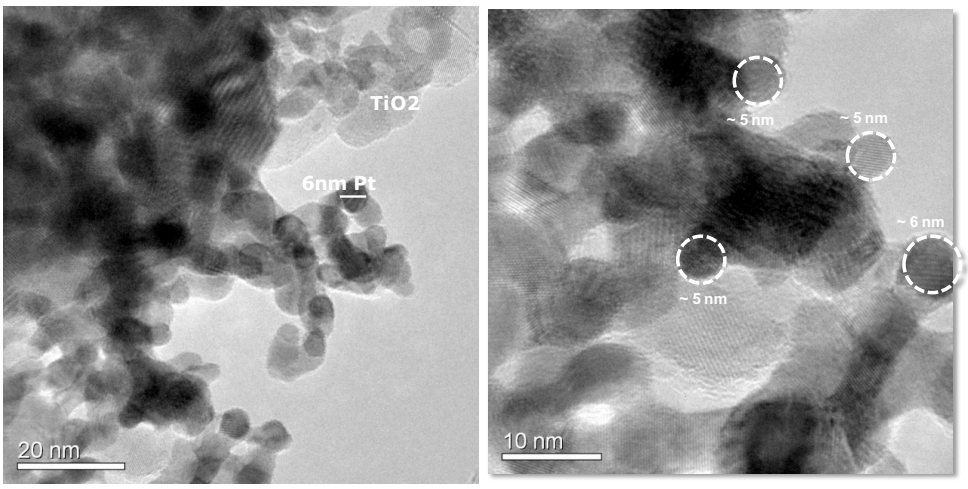

Figure 15. TEM micrographs of the Pt/TRO catalyst, showing Pt particles of size 4-6 nm.

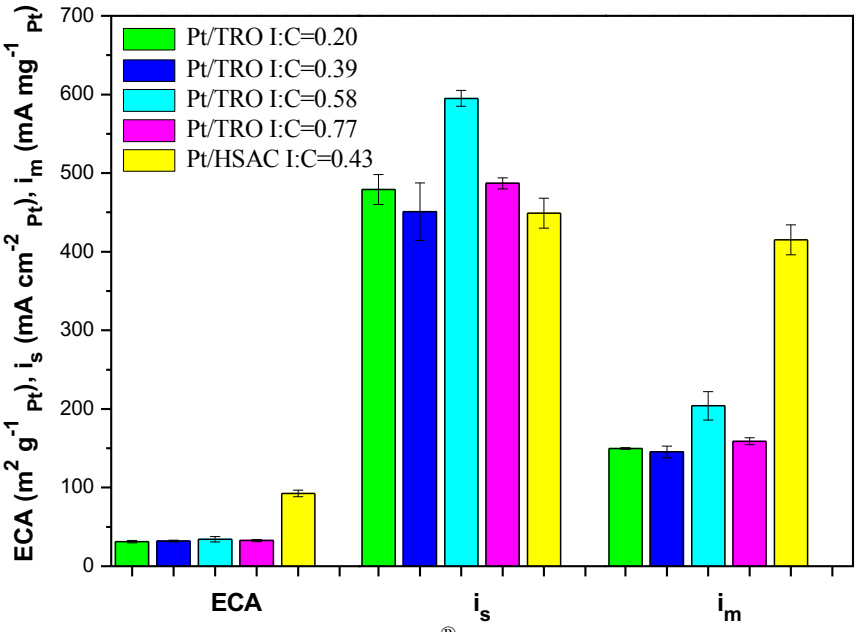

Figure 16. Optimization of ionomer (Nafion®) to catalyst weight ratio for 40% Pt/TRO. Baseline: ECA, specific activity (i_s) and mass activity (i_m) for Pt/HSAC at an optimal I/C ratio of 0.43. The CV and LP experiments used to extract this data were performed *ex-situ* in an RDE.

The 40%Pt/TRO catalyst was tested with various ionomer to catalyst (I/C) ratios to ascertain the optimal I/C ratio. Since the density and surface properties of TRO were quite different from that of carbon, it was assumed that the optimal I/C ratio would also differ. The optimal I/C ratio for 40%Pt/TRO was estimated to be 0.58. With this formulation the 40%Pt/TRO catalyst achieved the highest ORR mass and specific activities (**Figure 16**).

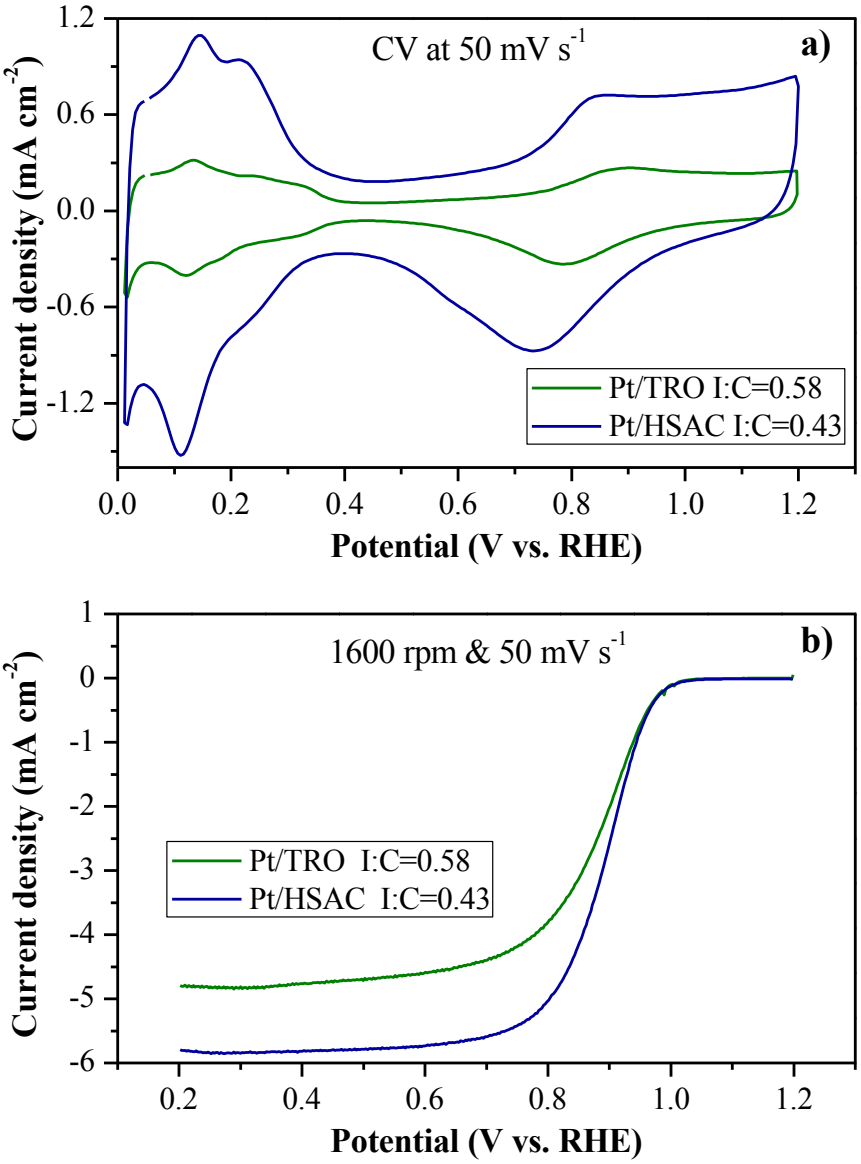

Figure 17. **(a)** Cyclic voltammograms in nitrogen degassed 0.1M perchloric acid for 40% Pt/TRO and 50% Pt/HSAC, and **(b)** ORR polarization curves obtained in oxygen saturated 0.1M perchloric acid for these catalysts. The Pt/HSAC catalyst was tested using an ionomer to catalyst weight ratio (I/C) of 0.43, and the Pt/TRO at the optimal I/C ratio of 0.58.

The 40%Pt/TRO catalyst showed similar H_2 adsorption and desorption characteristics encountered in Pt/HSAC catalysts when tested using CV (**Figure 17** a), but had lower ECA (from CV) and limiting current [from linear polarization experiments, **Figure 17** b] than the Pt/HSAC catalyst. The lower ECA was attributed to the larger Pt particle size, while the lower limiting current was attributed to mass transfer resistances within the catalyst layer resulting from non-optimized pore structure.

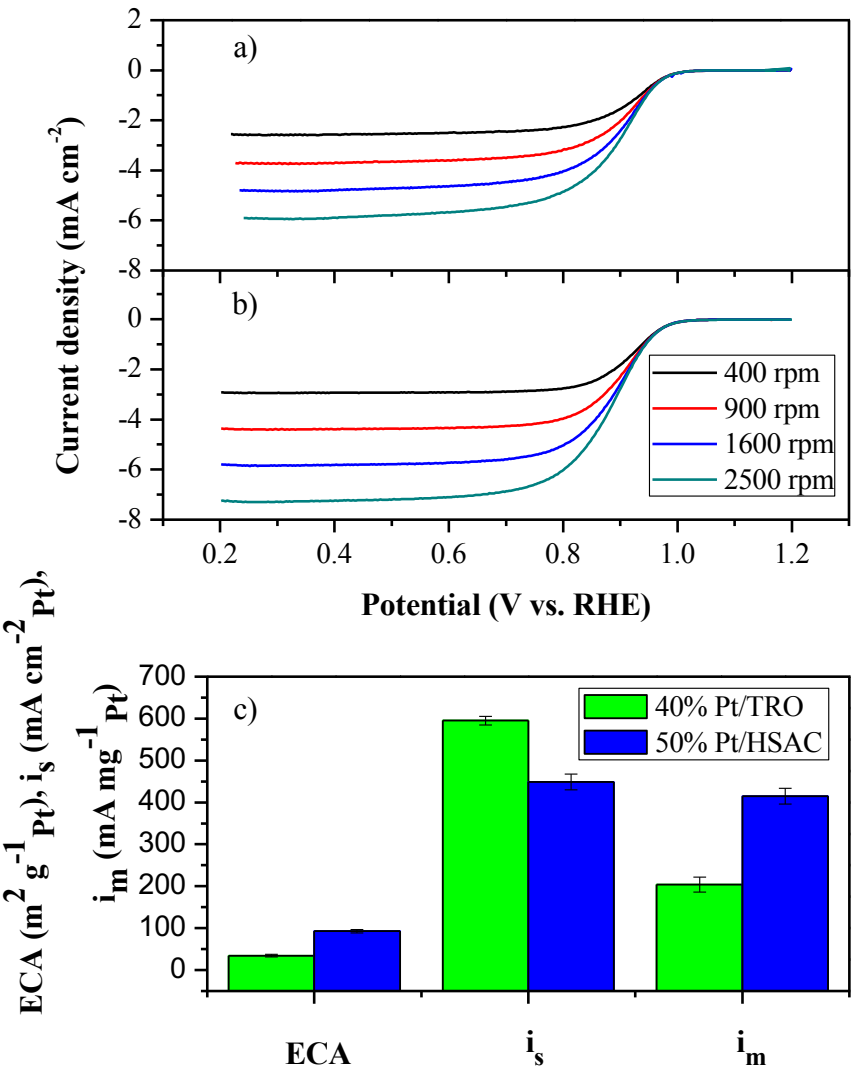

Figure 18. **a)** ORR LP curves for 40%Pt/TRO at various rotation rates, **b)** ORR LP curves for 40%Pt/TRO, and **c)** comparison of ECA and activity towards the ORR of 40%Pt/TRO and 50%Pt/HSAC catalyst. RDE experiments were performed in 0.1M $HClO_4$ at 60°C; nitrogen degassed for measuring the ECA, and oxygen saturated for determination of ORR activities.

The ORR activity for the 40%Pt/TRO catalyst was evaluated in an RDE using an optimized I/C ratio of 0.58g/g. Likewise, the baseline commercial Pt/HSAC catalyst was evaluated at its optimal I/C ratio of 0.43 g/g. **Figure 18** a&b shows the linear polarization curves at various rotation rates for the 40%Pt/TRO (a) and 50%Pt/HSAC (b) catalysts. From these polarization curves, the Levich and Koutecky-Levich (K-L) plots were prepared, and are shown in **Figure 19** and **Figure 20**. The K-L plot was prepared for potentials ranging 0.82 to 0.92 V vs. RHE, with the primary objective being to determine the number of electrons transferred and the kinetic currents at various overpotentials. The average number of electrons transferred (obtained using Levich equation) was 3.9 for Pt/HSAC and 3.2 for the Pt/TRO catalyst. The Tafel slopes calculated from the kinetic

currents extracted from the K-L plot (in the potential range 0.82 to 0.92 V vs. RHE) were 80 and 94 mV/decade for Pt/HSAC and Pt/TRO, respectively (**Figure 19** and **Figure 20**).

As shown in **Figure 19**, the ECA of 40% Pt/TRO was ca. 38 m^2/g_{Pt} (about 40% of the value obtained with Pt/HSAC). The lower ECA, arising primarily from larger Pt particle size, contributed to the higher specific activity observed in 40%Pt/TRO compared to 50%Pt/C (575A/m^2_{Pt} vs 525A/ m^2_{Pt}). The mass activity of 40% Pt/TRO was ca. 220 mA/mg_{Pt} (again, about 40% of the value obtained with Pt/HSAC). The lower mass activity was consistent with the larger Pt particle sizes (ca. 6 nm) in 40%Pt/TRO compared to 2.5-3 nm in Pt/HSAC. The larger particle size implied poorer platinum dispersion, yielding a lower number of Pt surface atoms relative to (unused) bulk atoms, thereby necessitating the use of a larger amount of catalyst to achieve a given turnover.

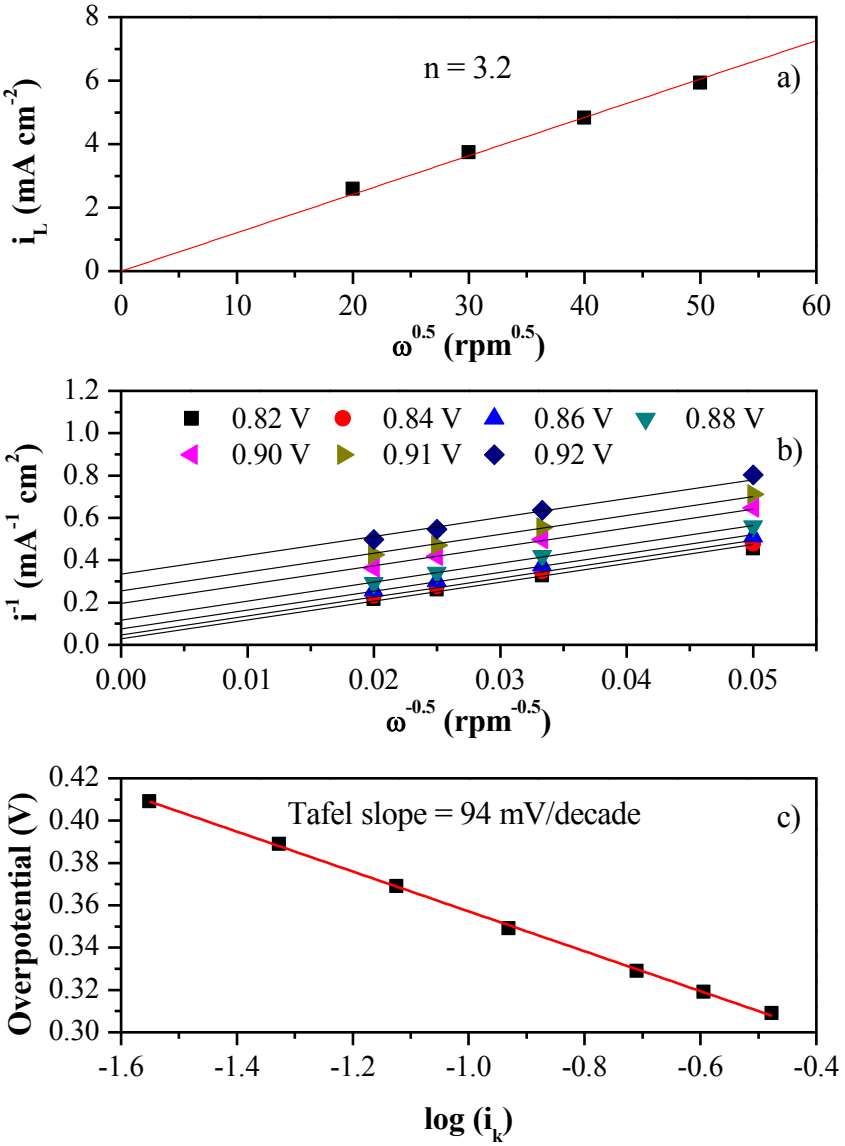

Figure 19. a) Levich plot showing the number of electrons transferred, Koutecky-Levich (K-L) plot, and b) Tafel slope (obtained from the kinetic currents extracted from the K-L plot) for 40%Pt/TRO. RDE experiments were performed in oxygen saturated 0.1M $HClO_4$ at 60°C.

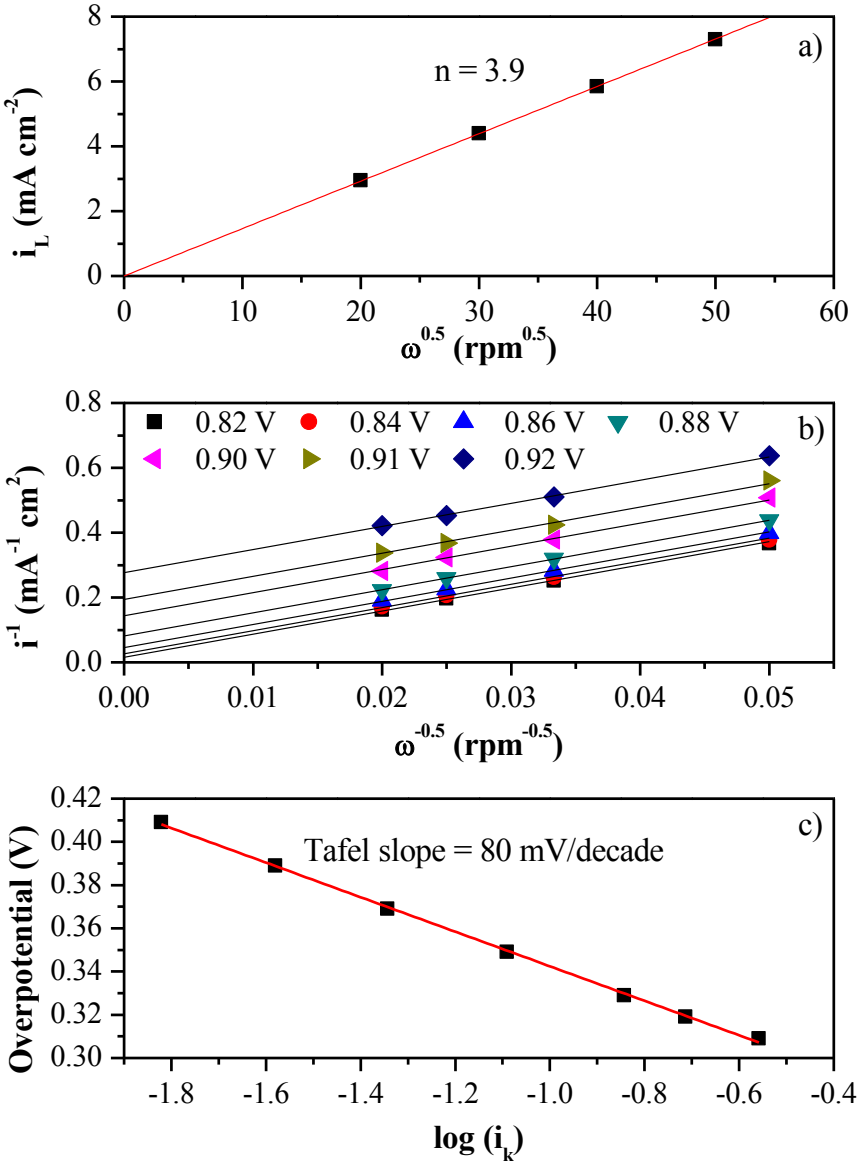

Figure 20. a) Levich plot showing the number of electrons transferred, b) Koutecky-Levich (K-L) plot, and b) Tafel slope (obtained from the kinetic currents extracted from the K-L plot) for 50%Pt/HSAC. RDE experiments were performed in oxygen saturated 0.1M $HClO_4$ at 60^{o}C.

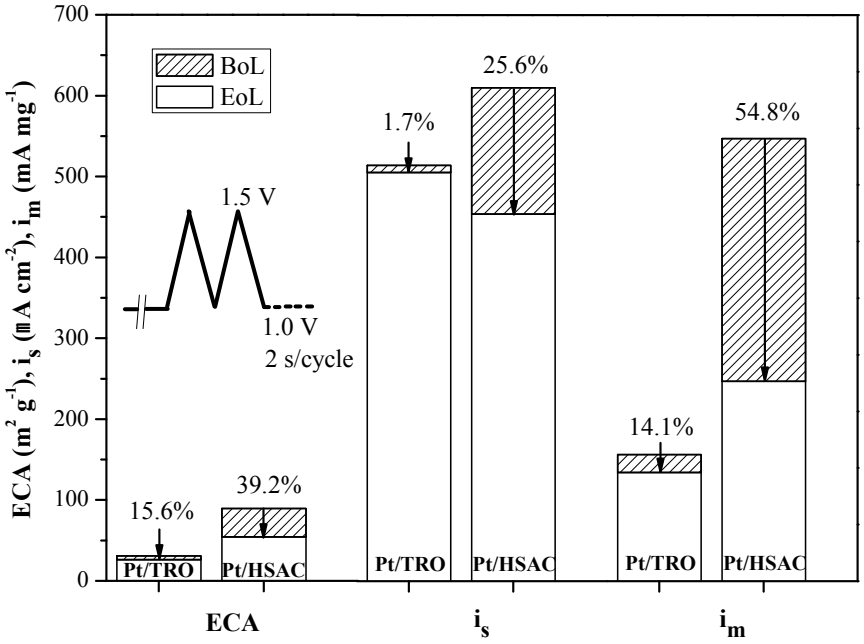

Figure 21. Comparison of ECA and ORR specific (i_s) and mass (i_m) activity for Pt/HSAC and Pt/TRO catalysts before (BoL) and after (EoL) the start-stop protocol (*ex-situ* experiments, performed on a RDE, in 0.1M $HClO_4$ electrolyte saturated with N_2 at 60^{o}C).

In-situ accelerated degradation tests were then performed on MEAs. **Figure 22** shows the polarization curves obtained (at 100% RH) on MEAs prepared with Pt/TRO and Pt/HSAC before and after exposure to the start-stop protocol, *in-situ*. There are two significant observations to note. First, despite the larger Pt particle size, and concomitantly lower ECA and mass activity as ascertained by *ex-situ* RDE tests, the Pt/TRO electrocatalyst yielded an initial MEA performance nearly identical to that obtained with an established benchmark (please note that this benchmark performance is very much in line with industry standards and is among the best available today). This indicated that the Pt/TRO catalyst was very much viable in terms of catalytic activity and performance. Second, and even more significantly, while the Pt/HSAC MEA revealed a very significant (and most likely catastrophic) loss in performance, the Pt/TRO showed minimal loss in performance upon exposure to 1000 start-stop cycles. The loss in cell voltage at 1A/cm^2 at 100% RH was almost 700 mV for Pt/HSAC whereas it was only ca. 15 mV for Pt/TRO. 40% RH data, shown in **Figure 23**, revealed a similar trend in terms of stability – exceptional stability for Pt/TRO as opposed to very poor stability for Pt/HSAC. These observations were attributed to the much higher stability of the TRO support compared to HSAC. MEAs prepared with each catalyst were then exposed to the load cycling protocol. While a significant loss in ECA was observed in each case, consistent with platinum dissolution and agglomeration, there was minimal impact on performance.

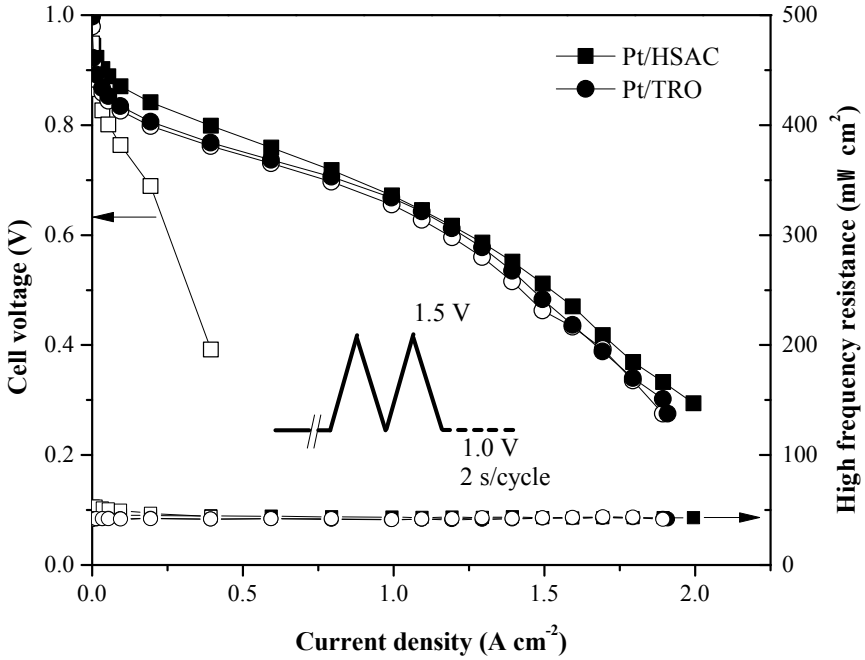

Figure 22. Comparison of fuel cell performance obtained with commercial Pt/HSAC and Pt/TRO before and after exposure to the start-stop protocol (1000 cycles). Experiment performed in a 25cm^2 single fuel cell at 80^{o}C and 100% RH. Anode: 0.40 mg Pt/cm^2; cathode: 0.35 mg Pt/cm^2; membrane: Nafion® 211. Closed symbols: beginning of life (BoL); Open symbols: end of life (EoL).

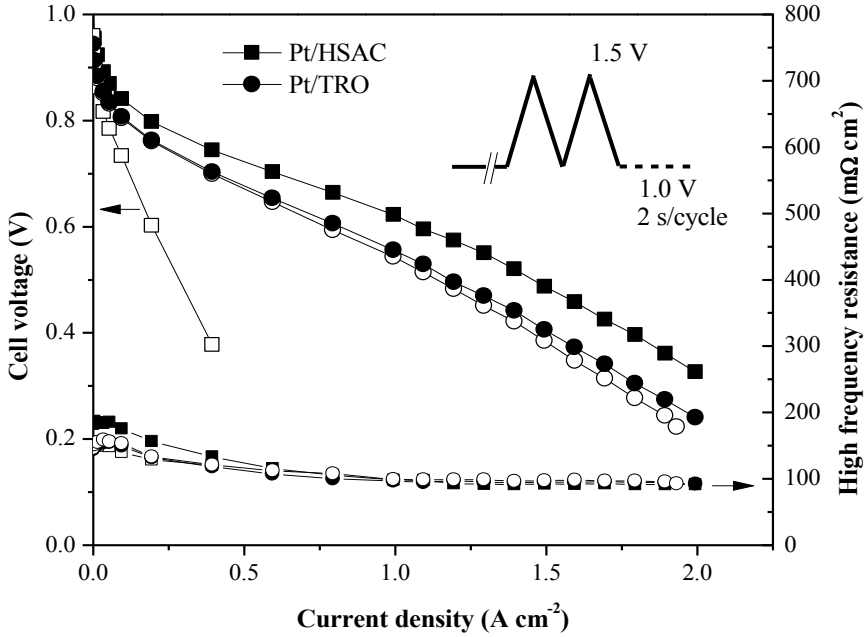

Figure 23. Fuel cell performance of 40% Pt/TRO and Pt/HSAC before and after exposure to the start-stop protocol for 1000 cycles. This *in-situ* test was carried out in a 25cm^2 single fuel cell at 80^{o}C and 40% relative humidity. Catalyst loadings: Anode: 0.40 mg Pt/cm^2; cathode: 0.35 mg Pt/cm^2; I/C ratios: Optimal for each electrode; Polymer electrolyte membrane: Nafion® 211. Closed symbols: beginning of life (BoL); Open symbols: end of life (EoL).

c

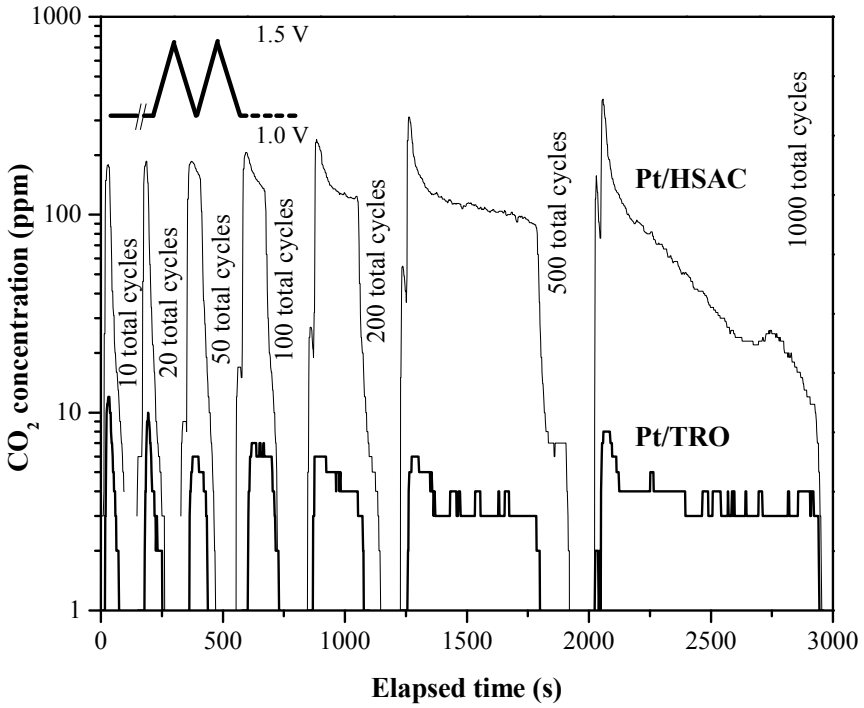

Figure 24. Evolution of carbon dioxide in the cathode exit stream during the *in-situ* support durability test (start-stop protocol) for Pt/HSAC and Pt/TRO.

3.7. Optimization of % Pt Loading and Ionomer Loading on Low Surface Area RTO Supports

3.7.1. Matching the Pt Particle Density of 30% Pt on Graphitized Ketjen Black (GKB)

A commercial 30% Pt/GKB catalyst would be a more appropriate comparison for the Pt/RTO catalyst since the GKB support has low surface area (relative to Ketjen Black and other high surface area carbons) and it has no micropores (pores < 2nm). The following calculations show that the target wt% of Pt for Pt/RTO should be 10%, in order to match the Pt particle density of 30% Pt/GKB.

From TEM measurements, the average diameter of Pt particles in 30% Pt/GKB is 5 nm, therefore the volume of 1 Pt particle would be:

$$\frac{4}{3}\pi r^3 = \frac{4}{3}\pi(2.5\times10^{-9}m)^3 = 6.54\times10^{-26}\ m^3\ \text{Pt} \qquad [1]$$

The surface area of 1 Pt particle would be:

$$4\pi r^2 = 4\pi(2.5\times10^{-9}\text{m})^2 = 7.85\times10^{-17}\ \text{m}^2\ \text{Pt} \qquad [2]$$

The mass ratio of Pt to carbon is:

$$\frac{0.3\text{g Pt}}{0.7\text{g Carbon}} = 0.43\ \frac{\text{g Pt}}{\text{g C}} \quad [3]$$

The density of Pt is 21.45 g/cm^3 so the volume of Pt per gram C is:

$$\frac{0.43\text{ g Pt}}{\text{g C}} \times \frac{1\text{ cm}^3\text{ Pt}}{21.45\text{ g Pt}} \times \frac{1\text{ m}^3\text{ Pt}}{100^3\text{ cm}^3\text{ Pt}} = 2.0\times10^{-8}\ \frac{\text{m}^3\text{ Pt}}{\text{g C}} \quad [4]$$

The number of Pt particles per gram of carbon would be:

$$2\times10^{-8}\ \frac{\text{m}^3\text{ Pt}}{\text{g C}} \times \frac{1\text{ Pt particle}}{6.54\times10^{-26}\text{ m}^3\text{Pt}} = 3.0\times10^{17}\ \frac{\text{Pt particles}}{\text{g C}} \quad [5]$$

The surface area of graphitized Ketjen Black (GKB) is 150 m^2/g so the number of Pt particles per m^2 C is:

$$3.0\times10^{17}\ \frac{\text{Pt particles}}{\text{g C}} \times \frac{1\text{ g C}}{150\text{ m}^2\text{ C}} = 2.0\times10^{15}\ \frac{\text{Pt particles}}{\text{m}^2\text{ C}} \quad [6]$$

Therefore, the 'roughness factor' or the ratio surface area of Pt/surface area of C is:

$$2.0\times10^{15}\ \frac{\text{Pt particles}}{\text{m}^2\text{ Pt}} \times \frac{7.85\times10^{-17}\text{ m}^2\text{ Pt}}{1\text{ Pt particle}} = \boxed{0.16\ \frac{\text{m}^2\text{ Pt}}{\text{m}^2\text{ C}}} \quad [7]$$

This 'roughness factor' obtained for Pt/GKB will have to be matched using the RTO support. Similar calculations were performed for the RTO support (39 m^2/g surface area).

The number of Pt particles per gram of RTO is:

$$2.0\times10^{15}\ \frac{\text{Pt particles}}{\text{m}^2\text{ RTO}} \times \frac{39\text{ m}^2\text{ RTO}}{1\text{ g RTO}} = 8.0\times10^{16}\ \frac{\text{Pt particles}}{\text{g RTO}} \quad [8]$$

The volume of Pt per gram of RTO would be:

$$8.0\times10^{16}\ \frac{\text{Pt particles}}{\text{g RTO}} \times \frac{6.54\times10^{-26}\text{ m}^3\text{Pt}}{1\text{ Pt particle}} = 5.2\times10^{-9}\ \frac{\text{m}^3\text{ Pt}}{\text{g RTO}} \quad [9]$$

Since the density of Pt is 21.45 g/cm^3, the necessary mass ratio of Pt to RTO is:

$$5.2\times10^{-9}\ \frac{\text{m}^3\text{ Pt}}{\text{g RTO}} \times \frac{21.45\text{ g Pt}}{1\text{ cm}^3\text{ Pt}} \times \frac{100^3\text{ cm}^3\text{ Pt}}{1\text{ m}^3\text{ Pt}} = 0.11\ \frac{\text{g Pt}}{\text{g RTO}} \quad [10]$$

Therefore, the target Pt wt.% for Pt/RTO where RTO has a surface area of 39 m^2/g should be:

$$\frac{0.11\text{g Pt}}{1.11\text{ g Pt/RTO}} = 10\%\text{ Pt} \quad [11]$$

3.7.2. Optimization of Ionomer Content of the Pt/RTO Catalyst Layer

The ionomer/support (I/S) weight ratio that was used in formulating the inks during MEA testing for both 40% Pt/RTO and 50% Pt/Ketjen Black (KB) was kept constant. Due to the disparity in the surface areas of the two supports (39 m^2/g for RTO vs. 800m^2/g for KB), it is expected that the volumetric ionomer coverage and hence, the ionomer film thickness covering the Pt particles will be significantly different.

In this part of the work, we calculated the target or appropriate ionomer content for a Pt/RTO catalyst layer using Pt/GKB as a reference. The ionomer film thickness could be estimated by dividing the volume of Nafion® ionomer (calculated from the mass of Nafion dispersed in the ink and the known density of Nafion) by the effective surface area (A_{eff}) of the catalyst. The effective surface area would be the area over which Nafion® could spread over, and it is taken to be equal to the measured BET surface area since both RTO and GKB are non-microporous supports (it is known that Nafion® would not be able to penetrate micropores (pores < 2nm) such as those found in high surface area Ketjen Black carbon). The dry thickness of the ionomer (σ) mixed with the Pt/GKB or Pt/RTO catalyst can be estimated using (Ignaszak and Gyenge, 2009):

$$\sigma \text{ (in cm)} = \frac{V_{Nafion}}{A_{eff}} = \frac{V_{Nafion®}}{A_{eff} \cdot 10^4 \cdot mass_{catalyst}} \quad [12]$$

where V_{Nafion} is the Nafion® volume (cm^3), A_{eff} is the effective area covered by Nafion® (cm^2), and A_{BET} (m^2/g) is the surface area of the catalyst. Using this formula, we have determined that in order to match the estimated ionomer film coverage for a 30% $Pt/GKB_{150m2/g}$ electrode with a nominal I/S weight ratio of 1.3, the target I/S weight ratio for a 10 wt% Pt on $RTO_{39\ m2/g}$ (as determined from the previous section) would be ~ 0.25.

10wt% Pt/RTO catalyst was prepared at NTCNA and tested in RDE (**Figure 25**). The ECA for the 10% Pt/RTO sample was 54 m^2/g, 50% higher than the value obtained for 40% Pt/RTO (only ~ 35 m^2/g). This indicates that the dispersion of Pt on the low surface area RTO support is better for the 10% sample such that more Pt active area is exposed and accessible. Furthermore, this ECA matches the value obtained for a 50% Pt/GKB catalyst (55 m^2/g, NTCNA in-house RDE data), which indicates that the goal of matching the Pt particle density of a Pt/GKB sample may have been achieved.

We then proceeded to prepare a catalyst ink of the 10% Pt/RTO catalyst which contained the target amount of ionomer based on an I/S weight ratio of 0.25. This ink has been successfully sprayed on 25 BCH GDL (SGL Carbon) at a Pt loading of 0.35 mg/cm^2 using NTCNA's automated robotic spray system. At this stage, we believe that the Pt/RTO catalyst is clearly superior to Pt/ITO in the MEA and hence will henceforth only work with this variant.

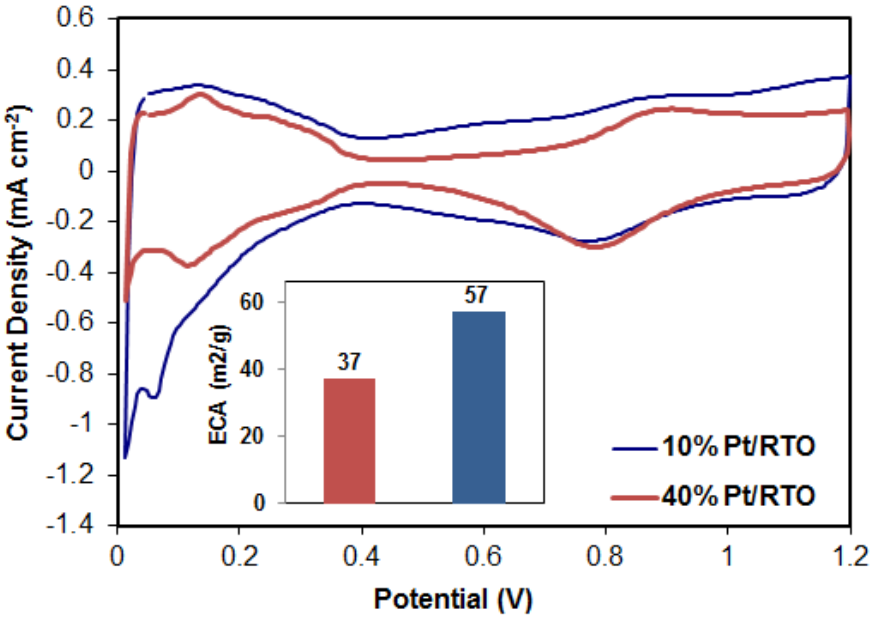

Figure 25. CV and ECS for 10 wt% and 40 wt% Pt/RTO electrocatalysts.

Our calculations show that the target Pt wt.% for Pt/RTO where RTO has a surface area of 39 m^2/g should be 10 wt% in order to match the Pt particle density of 30% Pt/GKB. 30% Pt/GKB (Graphitized Ketjen Black) would be a good comparison for Pt/RTO since both GKB & RTO have low surface areas and low microporosity (almost no pores < 2nm). We have also determined that in order to match the estimated ionomer film coverage for a 30% $Pt/GKB_{150m2/g}$ electrode with a nominal I/S weight ratio of 1.3 (typical value), the target I/S weight ratio for a 10 wt% Pt on $RTO_{39\ m2/g}$ would be ~0.3.

10wt% Pt/RTO catalyst were prepared and characterized. **Figure 26** shows the TEM images of the catalyst. Pt particle dispersion on the RTO support is qualitatively improved (less Pt agglomeration) as Pt loading is decreased from 40 to 10%. We then prepared a catalyst ink of the 10% Pt/RTO catalyst, which contained the target amount of ionomer based on an I/S weight ratio of 0.3. This ink was sprayed on 25 BCH GDLs (SGL Carbon) at a Pt loading of 0.35 mg/cm^2 using NTCNA's automated robotic spray system. We finished MEA testing and measurement of catalyst layer properties and the results are presented in this report.

As shown in **Figure 27**, the ECA for the 10% Pt/RTO sample was 45 m^2/g, higher than the value obtained for 40% Pt/RTO (at only 26 m^2/g). This indicates that the dispersion of Pt on the low surface area RTO support is better for the 10% sample such that more Pt active area is exposed and accessible. This is supported by the MEA tests in H_2/O_2 (as shown in the figure) where the 10% Pt/RTO catalyst had a higher mass activity than the 40% sample. **Figure 28** shows the SEM micrographs of the catalyst layers. The 10% Pt/RTO was ~ 15 microns thick, nearly 3 times thicker than the 40% sample. Based on this information, the calculated ionomer volume fraction is 0.7 and 0.4 for the 40% and 10% Pt/RTO catalyst layers, respectively. We also estimated the thickness (σ) of the

ionomer mixed with the catalyst by dividing the volume of Nafion by the effective catalyst surface area (A_{eff}) of the catalyst, the area over which Nafion could spread. The estimated Nafion film thickness is 7.2 and 3.3 for the 40% and 10% Pt/RTO catalysts, respectively. The ionomer volume fraction for the 10% Pt/RTO and the estimated ionomer film thickness are now closer to the values obtained for typical Pt/C cathodes.

The iV performance in H_2/Air is shown in **Figure 29**. Unfortunately, the performance of the 10% Pt/RTO was lower than the 40% sample. The HFR was also significantly higher for the 10% Pt/RTO. We have determined that the increase in HFR is not due to the decrease in ionomer content since several previous MEA tests has showed that decreasing the ionomer content does not lead to such drastic increases in HFR. Furthermore, as shown in **Figure 29** (right), the 10% Pt/RTO catalyst regardless of I/S ratio shows an HFR of around 100 $m\Omega \cdot cm^2$, about twice as high as the typical HFR of ~55 $m\Omega \cdot cm^2$. This led us to believe that the HFR increase is caused by the decrease in Pt wt. % from 40% to 10%.

Our hypothesis is that decreasing the Pt wt. % down to 10% on RTO may have decreased the electronic conductivity of the catalyst. RTO is a mixed metal oxide consisting of RuO_2 and TiO_2 phases. If some fraction of Pt particles are anchored on the TiO_2 phase, they could become electronically isolated (**Figure 30**). Furthermore, we have learned from our previous experience in MEA testing of different types of catalysts (e.g. commercial Pt/SnO_2, etc., outside of the scope of this project), that samples with less than ideal electronic conductivity show a characteristic HFR during MEA testing of around > 100 $m\Omega \cdot cm^2$.

We performed H_2/N_2 EIS analyses in order to determine the H^+ transport properties of the Pt/RTO catalyst layer, and the results are shown in **Figure 31**. The catalyst layer electrolyte resistance ($R_{H+,\ cath}$) for the 10% Pt/RTO cathode is not that much higher compared to the 40% Pt/RTO cathode (160 $m\Omega \cdot cm^2$ vs. 90 $m\Omega \cdot cm^2$, respectively). Moreover, taking into account the catalyst layer thickness and ionomer volume fraction, the calculated H^+ conductivity ($\sigma_{H+,\ cathode}$) for both cathodes are comparable (0.009 vs. 0.006 mS/cm for 10% and 40% Pt/RTO, respectively). Our hypothesis that the 10% Pt/RTO has lower electronic conductivity is also supported by the HFR obtained in H_2/N_2 EIS measurements where the 10% Pt/RTO sample had more than double the high frequency resistance value of the 40% sample. This can be easily seen in the Nyquist plot by comparing the x-axis intercepts of the two curves.

Figure 32 shows the H_2/Air and H_2/O_2 iV performance of 10% Pt/RTO vs. 40% Pt/RTO. The 10% Pt/RTO MEA has lower iV performance due to ohmic losses (poor electronic conductivity). The HFR-corrected H_2-O_2 iV performance is identical for both MEAs, and higher ECA and mass activities are obtained with 10% Pt/RTO.

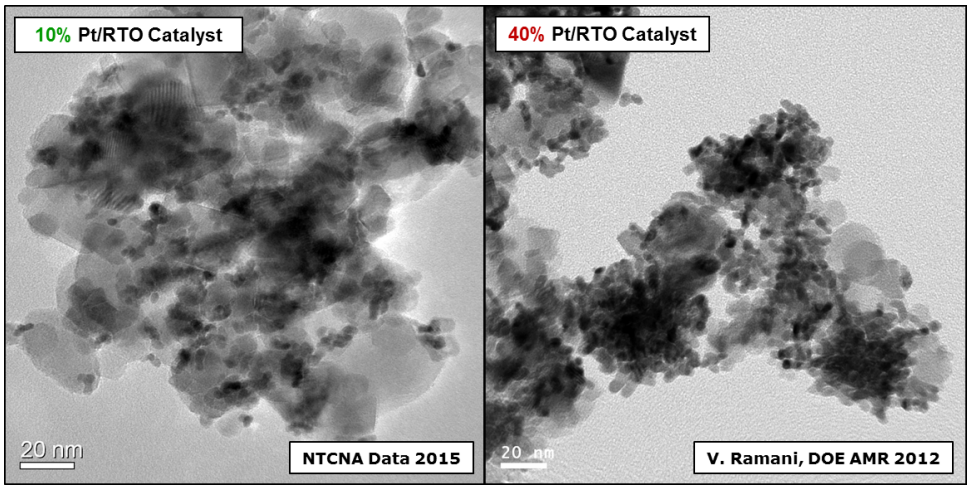

Figure 26. TEM Micrographs of 10% Pt/RTO versus 40% Pt/RTO. Pt particle dispersion on the RTO support is qualitatively improved (less Pt agglomeration) as Pt loading is decreased from 40 to 10%.

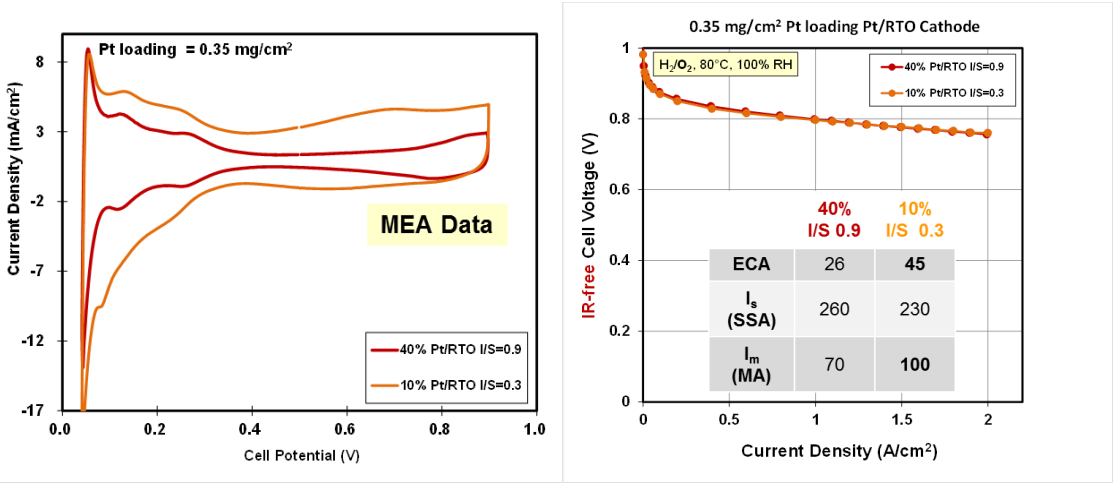

Figure 27. MEA CVs of 10% Pt/RTO versus 40% Pt/RTO and H_2/O_2 MEA performance. The ECA for the 10% Pt/RTO sample was 45 m^2/g, higher than the value obtained for 40% Pt/RTO (at only 26 m^2/g). This indicates that the dispersion of Pt on the low surface area RTO support is better for the 10% sample (more Pt active area is exposed and accessible)

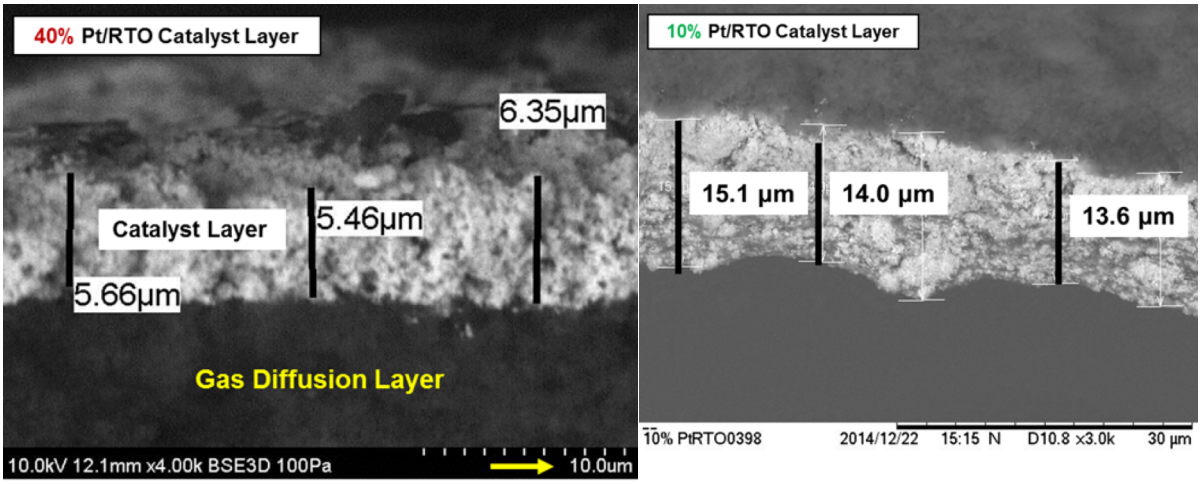

Figure 28. SEM micrographs of the 40% Pt/RTO and 10% Pt/RTO.

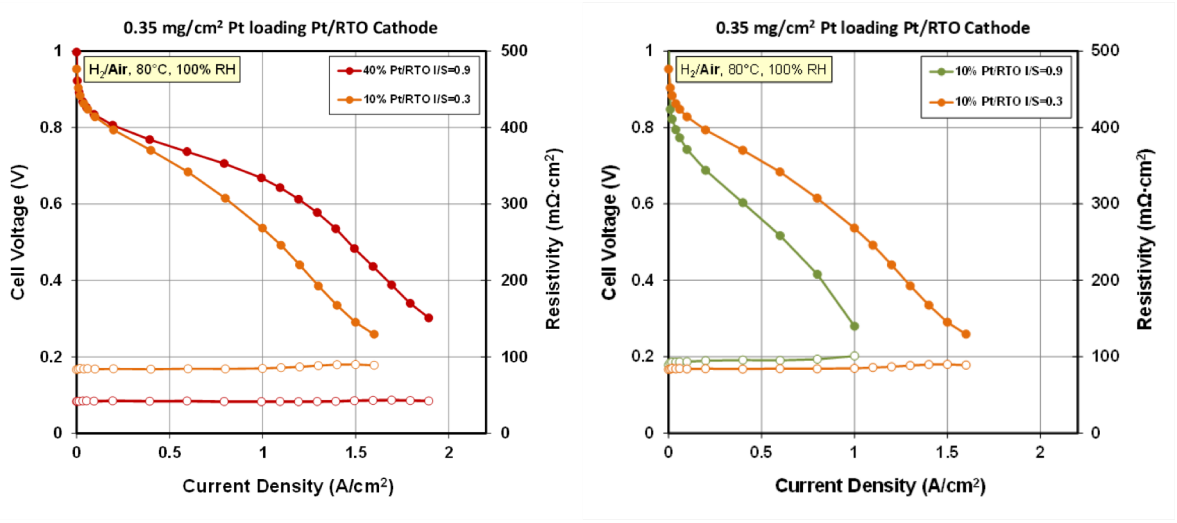

Figure 29. H_2/Air performance of 10% Pt/RTO (I/S=0.3) versus 40% Pt/RTO (I/S=0.9) (left) and 10% Pt/RTO with I/S=0.9 vs. I/S=0.3 (right). The increase in HFR is caused by the decrease in Pt loading from 40% to 10%.

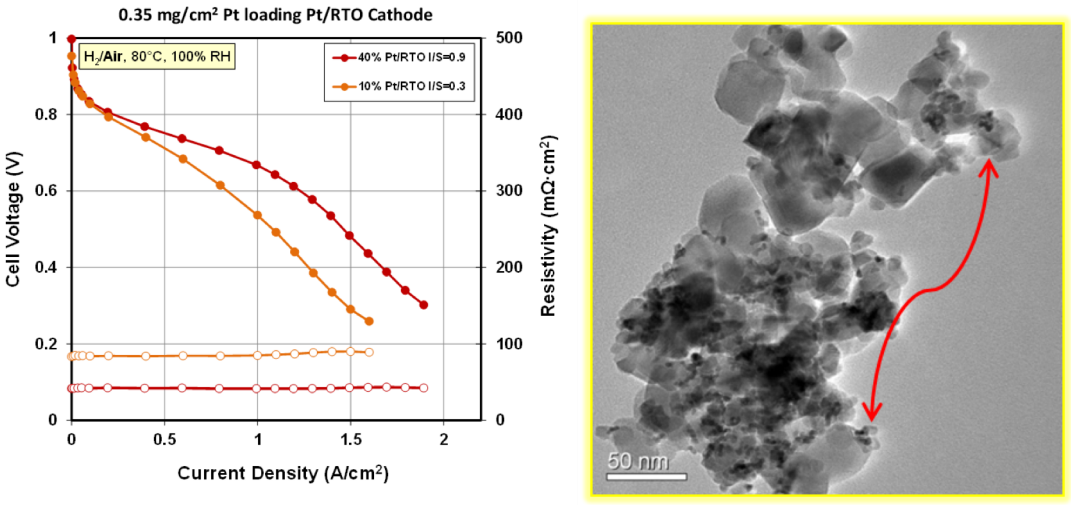

Figure 30. Based on the higher HFR of the 10% Pt/RTO sample, it is hypothesized that the catalyst has low electronic conductivity. RTO is a mixed metal oxide consisting of RuO_2 and TiO_2 phases so if some fraction of Pt particles are anchored on the TiO_2 phase, they could become electronically isolated. This hypothesis is supported by the TEM micrograph shown on the right, where the red arrow shows possible electronic isolation between Pt particles that are far apart and anchored on different phases (RuO_2 vs. TiO_2 phase) on the RTO support.

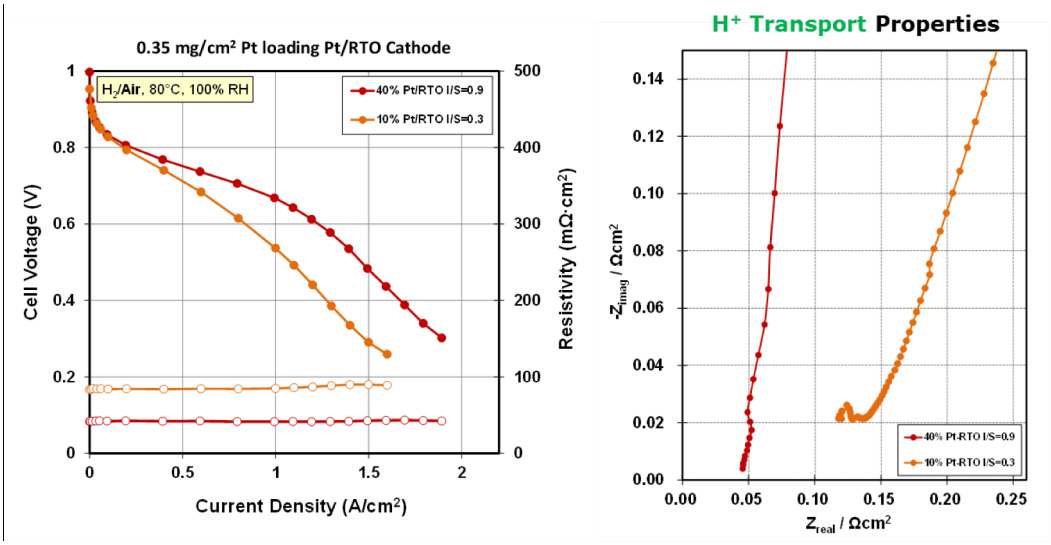

Figure 31. H_2/Air iV performance of 10% Pt/RTO vs. 40% Pt/RTO (left) and H_2/N_2 EIS analysis (Nyquist plot, right) used for determining the catalyst layer electrolyte resistance (R_{H+cath}).

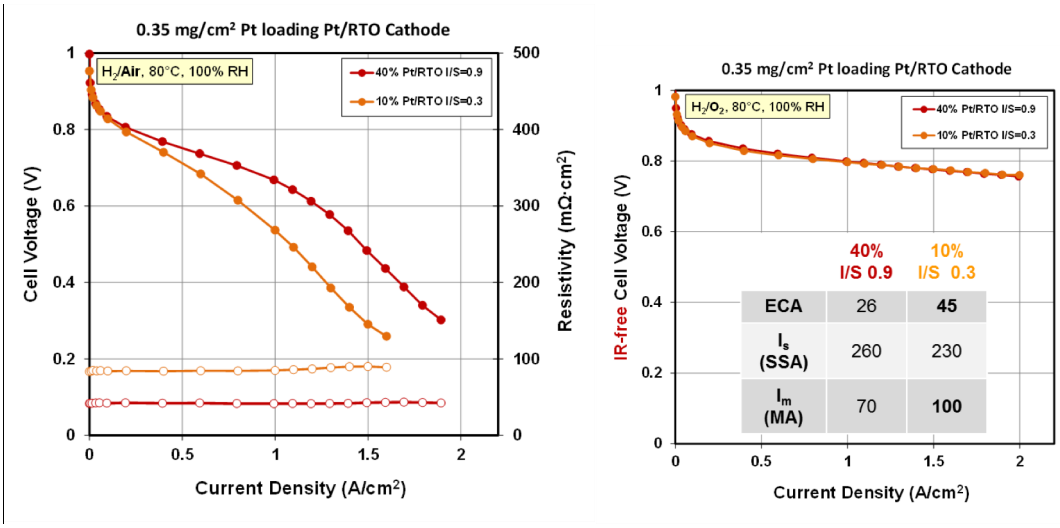

Figure 32. H_2/Air and H_2/O_2 iV performance of 10% Pt/RTO vs. 40% Pt/RTO. The 10% Pt/RTO MEA has lower iV performance due to ohmic losses (poor electronic conductivity). The HFR-corrected H2-O2 iV performance is identical for both MEAs, and higher ECA and mass activities are obtained with 10% Pt/RTO.

3.8. Analysis of Transport Properties of 40% Pt/HSAC and 10% Pt/RTO Electrocatalysts

This work was one at NTCNA in order to have a better understanding at the basic level of transport phenomena (reactants and products to/from the Pt active sites) in both commercial catalyst and Pt/RTO. The study starts with the observation Pt black (fuel cell grade) has significantly poorer iV performance compared to Pt/RTO and Pt/HSAC. In order to optimize the Pt/RTO catalyst and catalyst layer, we sought to obtain a better understanding of its microstructure and transport properties (See **Figure 33** and **Figure 34**). Limiting current measurements with dilute O_2 were performed in order to determine the O_2 gas transport resistance in the catalyst layer (RO_2, local). The details can be found in the papers of Nonoyama et al., 2011. The O_2 gas transport resistance, R_{other}, for the Pt/RTO catalyst layer is higher than that for Pt/HSAC (See **Figure 35**). This is consistent with the differences in the catalyst layer thickness, ionomer film thickness, Pt ECA, and effective ionomer area (ionomer covering Pt particles/agglomerates).

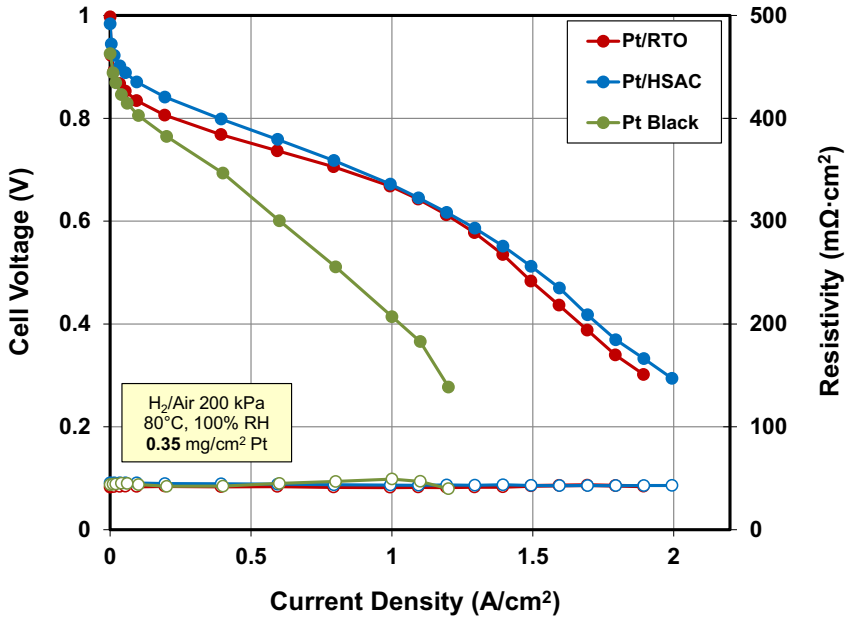

Figure 33. Comparison of fuel cell performance for Pt black, Pt/HSAC and Pt/TRO.

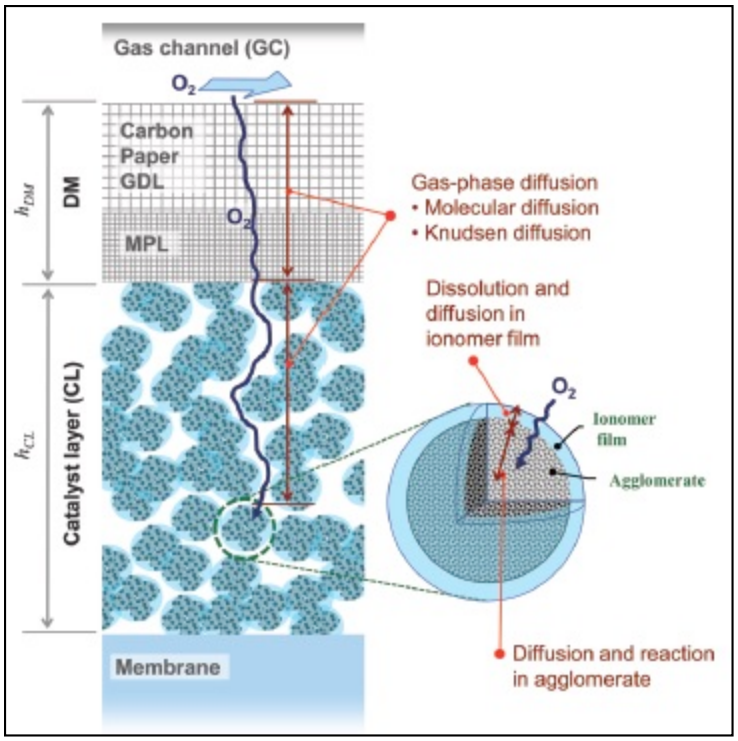

Figure 34. Scheme depicting the transport phenomena occurring in an operating PEMFC.

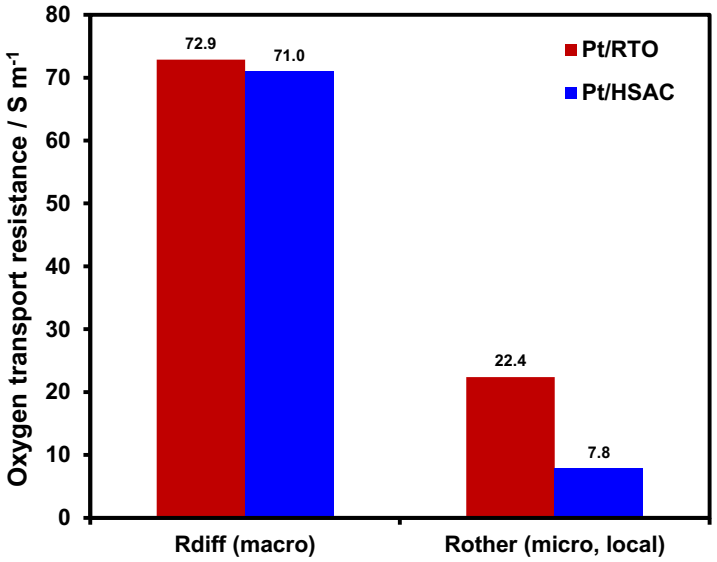

Figure 35. Comparison of transport resistances for commercial Pt/C (Pt/HSAC) and Pt/RTO.

3.8.1. Proton Resistance in the Catalyst Layer ($R_{ionomer}$) using H_2-N_2 EIS

We have investigated some transport properties of the Pt/RTO cathode catalyst layer (at a Pt loading of 0.35 mg/cm^2) and compared to conventional Pt/HSAC cathode, with the same Pt loading and ionomer/support weight ratio. The goals were to determine **1)** the proton resistance in the catalyst layer using EIS and **2)** the O_2 gas transport resistance of the catalyst layer.

The proton resistance ($R_{ionomer}$) in the catalyst layer of a Pt/RTO cathode catalyst layer was investigated using H_2/N_2 EIS based on the well-known method developed by Lefebvre et. al., 1999 and Makharia et. al. 2005. **Figure 36** shows the Nyquist plots for H_2/N_2 operation at 0.45V for Pt/RTO and Pt/HSAC cathodes having the same Pt loading of 0.35 mg/cm^2 and ionomer/support (I/S) mass ratio of 0.9. The calculated $R_{ionomer}$ for Pt/HSAC and Pt/RTO was 150 and 12 mΩ-cm^2, respectively. This shows that the Pt/RTO catalyst layer has about *an order or magnitude less proton transfer resistance* compared to the Pt/HSAC catalyst layer.

Since the ionomer/support ratio that was used in formulating the ink for both catalysts was the same (0.9), it is expected that the volumetric coverage of ionomer of both catalysts will be significantly different due to the disparity in the surface areas. The surface area of Pt/HSAC is ~ 800 m^2/g, while Pt/RTO has ~ 50 m^2/g, so the ionomer volumetric coverage and the ionomer film thickness on Pt/RTO is likely to be higher than for Pt/HSAC. This may explain the significantly higher proton conductivity (or lower proton resistance) in the Pt/RTO catalyst layer compared to Pt/HSAC.

3.8.2. O_2 Gas Transport Resistance Measurement

The oxygen gas transport characteristics of the Pt/RTO catalyst layer was investigated and compared to Pt/HSAC cathodes having the same Pt loading of 0.35 mg/cm^2 and ionomer/support (I/S) mass ratio of 0.9. The technique used in the analysis was based on the method developed by Mashio et. al., 2007. The method evaluates the oxygen gas transport in a fuel cell catalyst layer using limiting current measurements (low concentrations of O_2 diluted in N_2). The hypothesis behind the technique is that O_2 diffusivity in the catalyst layer might be found from the "other transport resistance", $\mathbf{R_{other}}$, which includes the Knudsen diffusion resistance, and the transport resistance through the ionomer film and liquid water. This R_{other} parameter is expected to be significantly affected by the catalyst layer structure, which is in turn, affected by the catalyst layer specifications, specifically the ionomer/carbon or ionomer/support weight ratio (I/C or I/S ratio)

The results of the gas transport analysis (**Figure 37**) shows that the R_{other} of the Pt/RTO catalyst layer is almost double that of the Pt/HSAC cathode. Due to the disparity in surface areas between Pt/HSAC and Pt/RTO, as discussed above, the ionomer volumetric coverage and the ionomer film thickness on Pt/RTO is likely to be higher than for Pt/HSAC since both catalyst layers had the same ionomer/support weight ratio of 0.9. This may explain the significantly higher R_{other} observed for Pt/RTO compared to Pt/HSAC. This result is consistent with known findings in the literature (Mashio et.. al., 2007) that the other transport resistance, R_{other}, increases with increasing I/C ratio for the same kind of catalyst.

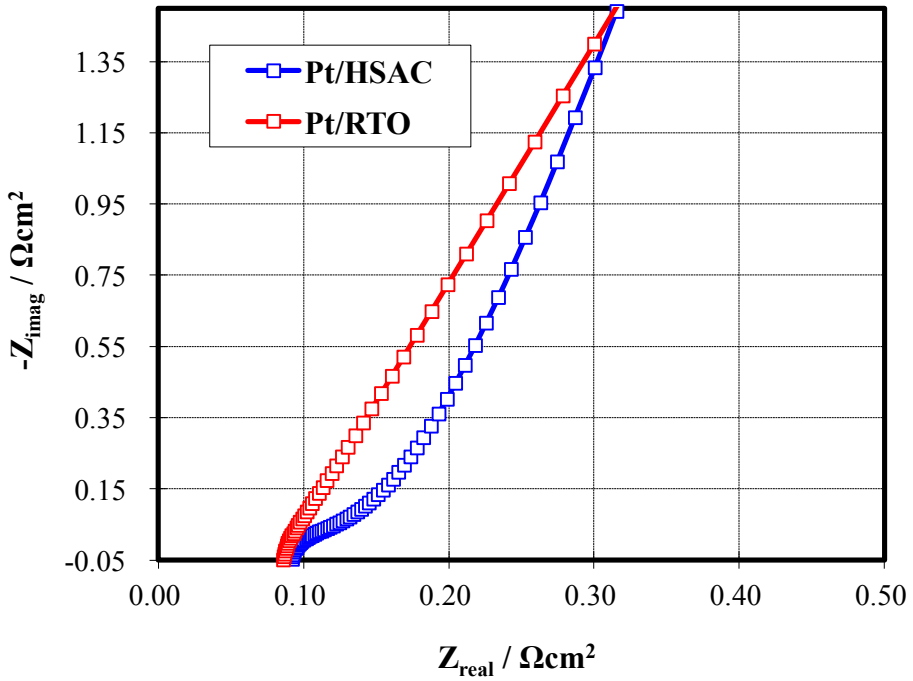

Figure 36. Nyquist plots for H_2/N_2 operation for Pt/RTO and Pt/HSAC cathodes having the same Pt loading of 0.35 mg/cm^2 and Ionomer/Support (I/S) mass ratio of 0.9. The calculated $R_{ionomer}$ for Pt/HSAC and Pt/RTO was 150 and 12 mΩ/cm^2, respectively. Cell conditions: 80°C, 100% RH

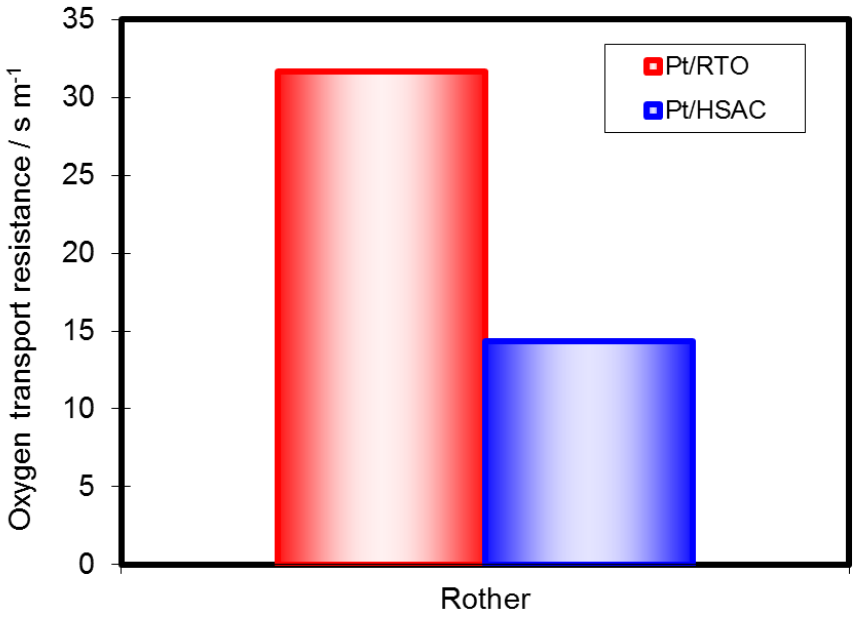

Figure 37. 'Other transport resistance', $\mathbf{R_{other}}$, for Pt/RTO and Pt/HSAC cathode catalyst.

4. Indium Tin Oxide Catalyst Support

Accomplishments

- RDE Testing of both 20% and 40% Pt/ITO showed mass activities of ~150 $mA/_{mgPt}$, comparable to Pt/RTO
- Pt/ITO was very stable under start-up/shutdown accelerated degradation protocol. The ECSA change was less than 4% over 10,000 cycles. The load cycling accelerated protocol (from 0.6 to 0.95 V vs. SHE) resulted in a loss of approximately 34% of the initial ECSA after 10,000 cycles.
- Great RDE results but not translated to MEA. ITO degrades under MEA conditions, shown by XPS
- A cost model for RTO, ITO supports has been developed and their durability benefits have been considered.

4.1. Preparation of High Surface Area ITO

The hydroxides were obtained by the co-precipitation method and dried using supercritical carbon dioxide. 2 g of indium nitrate was dissolved in the approximately 200 mL deionized water (0.04 mol/L). Then, 78 uL tin tetrachloride was added to the solution, and stirred for 20mins. A stock solution (0.5mol/L) of hexamethylenetetramine (HMT) in deionized water was prepared (14.019 g HMT dissolved in 200 mL H_2O) and added dropwise to the above mixture. The HMT hydrolyzes slowly, yielding ammonia and formaldehyde. The solution was stirred overnight (at room temperature) to allow complete precipitation of the hydroxides. Then, the precipitate was recovered by centrifugation, washed three times with DI water, another three times with isopropanol, and finally 5-8 times with acetone during 2-3 days to prepare for supercritical drying. The wet solid (in acetone) was dried using supercritical carbon dioxide. The ITO precursor (indium and tin hydroxides) obtained by supercritical drying method was heat treated at 820°C during 2.0-2.5h to obtain the ITO.

This ITO had higher surface area than the ITO obtained from the precursor dried in a conventional oven at 60°C. The BET surface area of the ITO precursor (using supercritical dryer) was higher than 200 m^2/g, and the surface area for the ITO (after heating at 820°C) was higher than 70 m^2/g. This was almost twice the BET surface area obtained with the previous method; the conductivity did not change.

Table 4. The comparison of commercial ITO and ITO made for this project

	Commercial ITO	**ITO from co-precipitation method**
Precursor surface area (m^2/g)	Not available	124± 2
ITO Surface area (m^2/g)	30± 2	45± 2
Conductivity (S/cm)	0.6-0.7	1.3± 0.1

4.2. Deposition of Platinum Nanoparticles on ITO by Chemical Reduction of Pt Precursor with Formaldehyde

0.14 g of the catalyst support was dispersed in approximately 150mL DI water. The pH value of the suspension was adjusted with $NaHCO_3$ to approximate 7. The mixture was stirred and sonicated for 1 hour to improve the dispersion and wetting of the support in the solution. Later 0.25g of H_2PtCl_6 was dissolved in 15 ml DI water and added dropwise to the stock solution using a burette. The mixture was stirred and sonicated for 2 hour to let the precursor to adsorb on the support surface. Then, 195 microliters of formaldehyde (37%) was dissolved in 1.95 mL of DI water and added to the suspension. The mixture was kept stirring overnight at 80^{o}C to complete the reduction of the Pt precursor. The solid materials containing the Pt nanoparticles deposited onto the non-carbon support was recovered by filtration, washed with abundant DI water, and dried in an oven at 60^{o}C. Finally, the catalyst was heated at 120 °C in air atmosphere overnight to improve the binding between the Pt particles and the ITO support.

4.3. Characterization of Support and Catalyst

X-ray diffraction (XRD) was performed using a Rigaku Miniflex diffractometer to confirm the structure and crystallite size of ITO. Diffractograms were recorded in the range of 2θ = 20° to 80° with a step of 0.6 degree/min. **Figure 38** and **Figure 39** show the XRD for ITO and 40%Pt/ITO. They display the expected diffraction pattern for those materials.

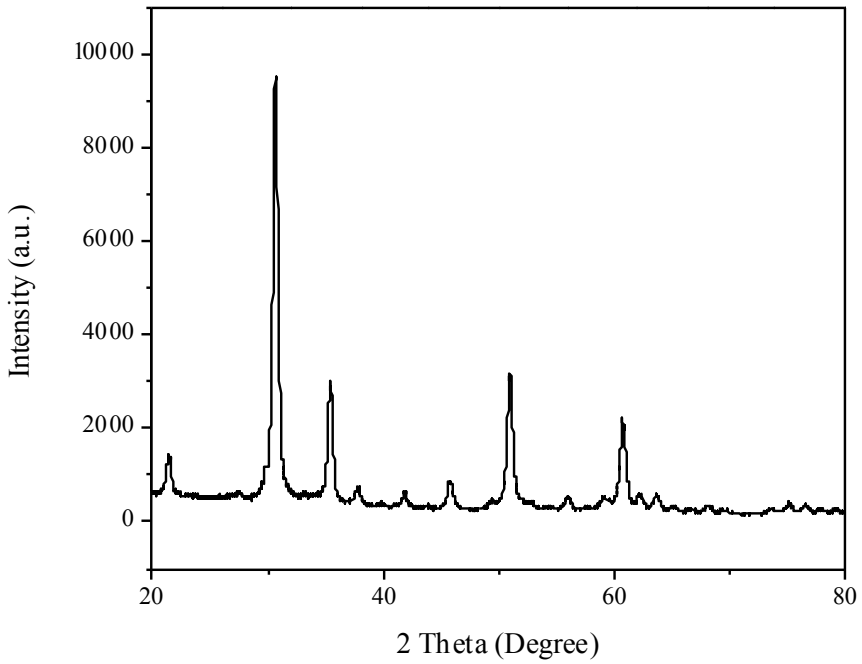

Figure 38. XRD pattern for ITO (heated under air atmosphere). The spectrum shows peaks clearly at 31°, 36°, 51° and 61° corresponding to (222), (400), (440) and (622) planes of ITO (cubic structure, JCPDS 06-0416). Crystallite size calculated using Debye-Scherrer equation was 22 nm.

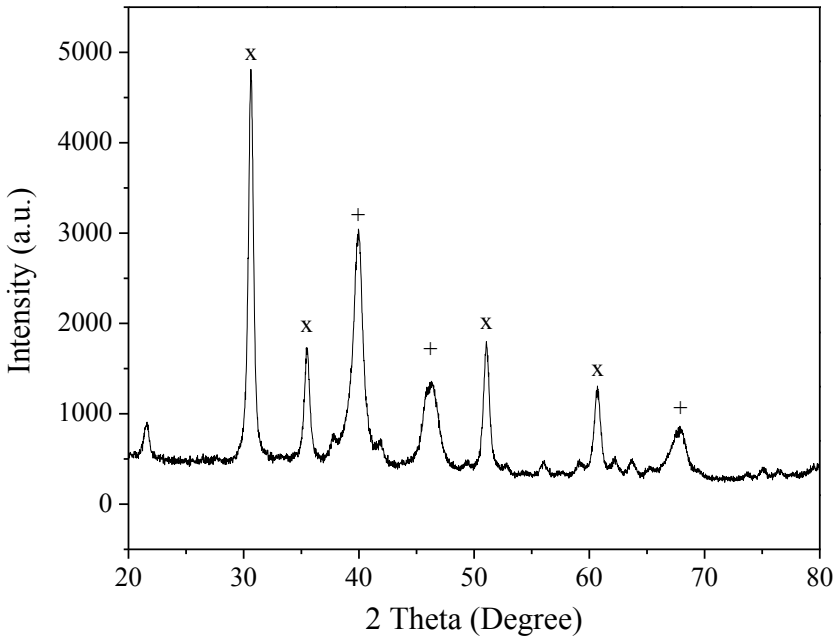

Figure 39. XRD pattern for 40% Pt/ITO. The spectrum shows peaks clearly at 31°, 36°, 51° and 61° corresponding to (222), (400), (440) and (622) planes of ITO (cubic structure, JCPDS 06-0416). Pt peaks at 40 °, 47 °, 68 ° (face-centered cubic) were also clearly visible. Crystallite size calculated using Debye-Scherrer equation were 7.7 nm for Pt and 22 nm for ITO particles.

Figure 40 shows a TEM micrograph of ITO support particles (no Pt). The powder particles appear as irregularly-shaped, mostly cube-like particles ranging from ~20 nm in size. A TEM image of a 50% Pt/ITO sample is shown in **Figure 41**. Good Pt dispersion is achieved despite the low surface area of the ITO support, and the Pt particle sizes are within 3-4 nm.

20wt% Pt on ITO support also synthesized to investigate the effect on Pt loading on mass activity. The CV, ECA, specific and mass activities for a 50% and 20% Pt on ITO sample are presented in **Figure 42**. The mass activity obtained for both catalysts are almost equal (140-150 mA/mgPt), and comparable to what we obtain for Pt/RTO and a commercial catalyst made by TKK, TEC10E50E-HT, which shows a mass activity of ~120 mA/mgPt.

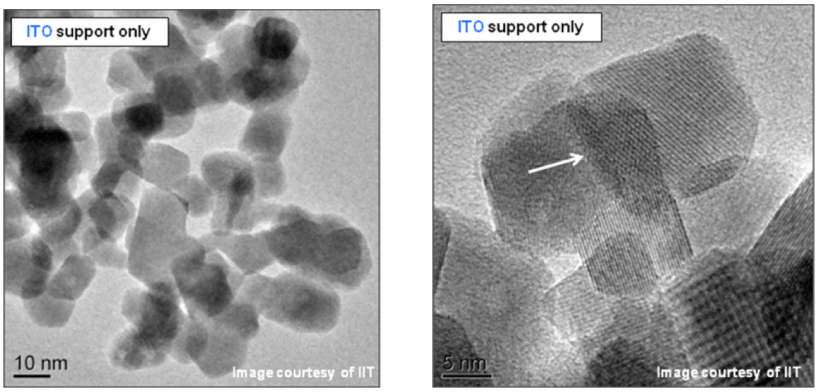

Figure 40. Representative TEM micrographs of ITO support particles. The support surface has several areas which are defect-free and highly crystalline.

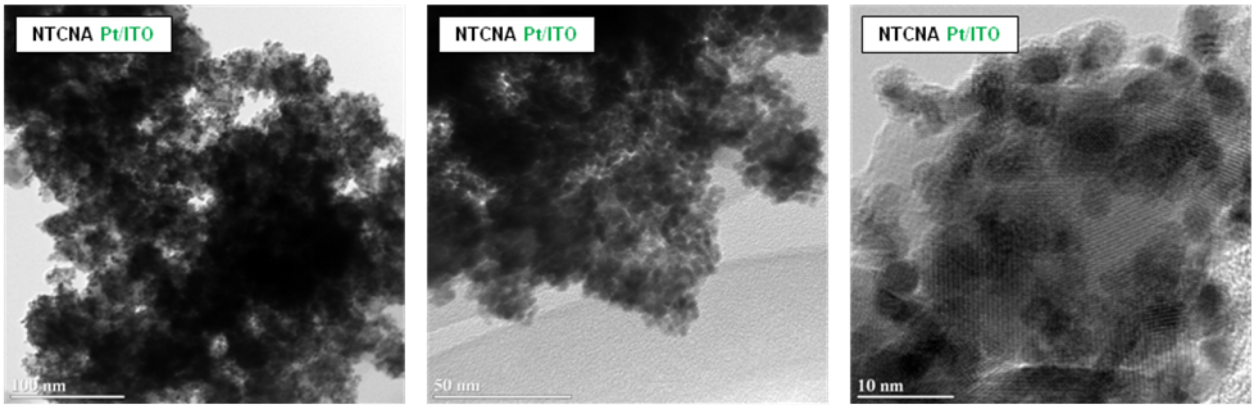

Figure 41. Representative TEM micrographs of a 50% Pt/ITO sample.

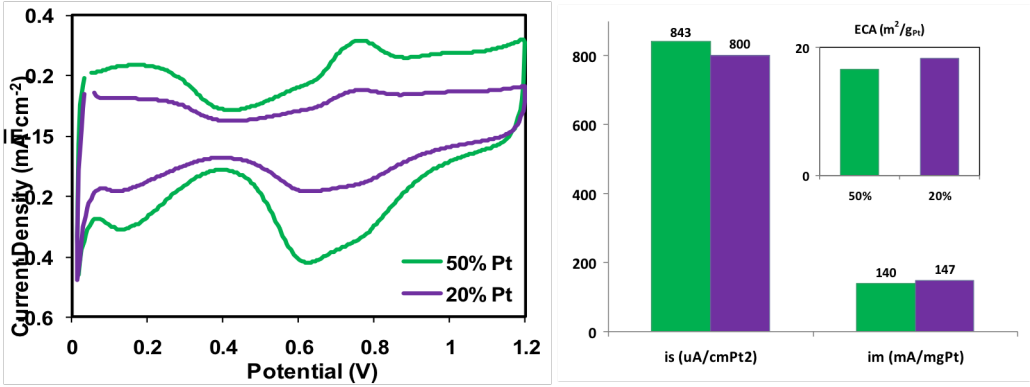

Figure 42. The CV, ECA, specific and mass activities for 50% and 20% Pt on ITO samples.

These results are similar to Pt/RTO catalyst showing similar mass activities for 20% catalyst and higher Pt loading catalysts. These results are very important in commercialization of these durable catalysts in PEM fuel cells as based on cost model catalyst cost is dominated by Pt cost. Reducing the Pt loading can help reduce the catalyst cost.

4.4. Electrochemical Stability for 40%Pt/ITO Catalyst Prepared by Reduction of $H_2PtCl_6 \cdot 6H_2O$ with Formaldehyde.

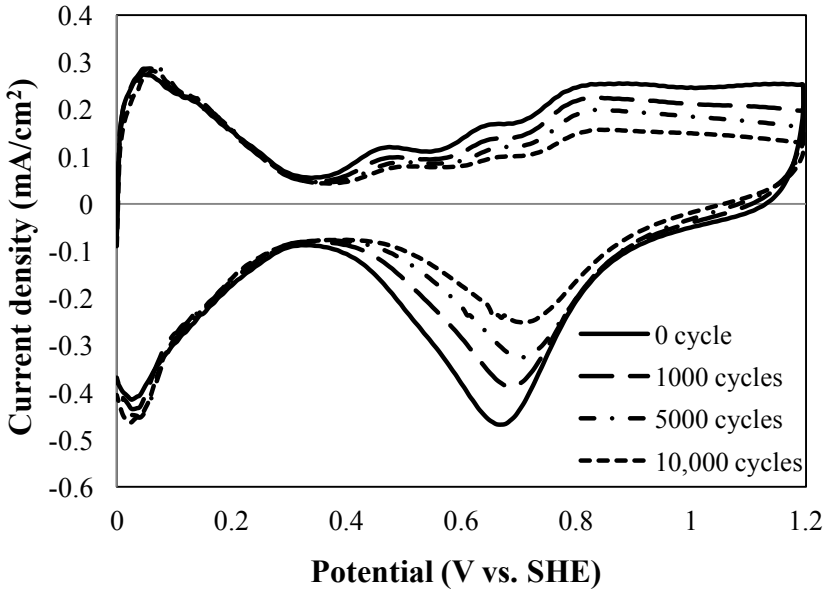

Figure 43. Cyclic voltammograms (at 20mV/s) of 40%Pt/ITO (formaldehyde reduction method) after 0, 1000, 5000 and 10,000 cycles (start-up/shut-down accelerated degradation protocol). RDE experiment was conducted at room temperature in nitrogen saturated 0.1M perchloric acid.

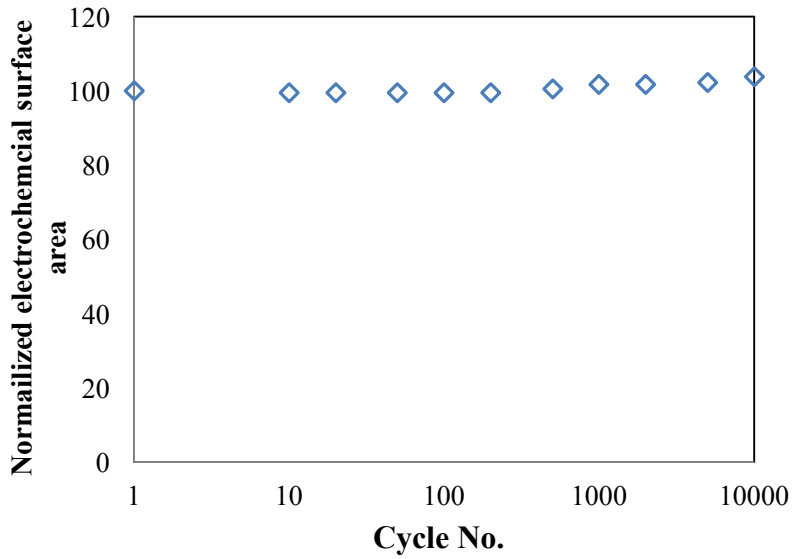

Figure 44. Normalized ECSA vs. cycle number for 40%Pt/ITO (formaldehyde reduction method) during start-up/shut-down accelerated degradation protocol.

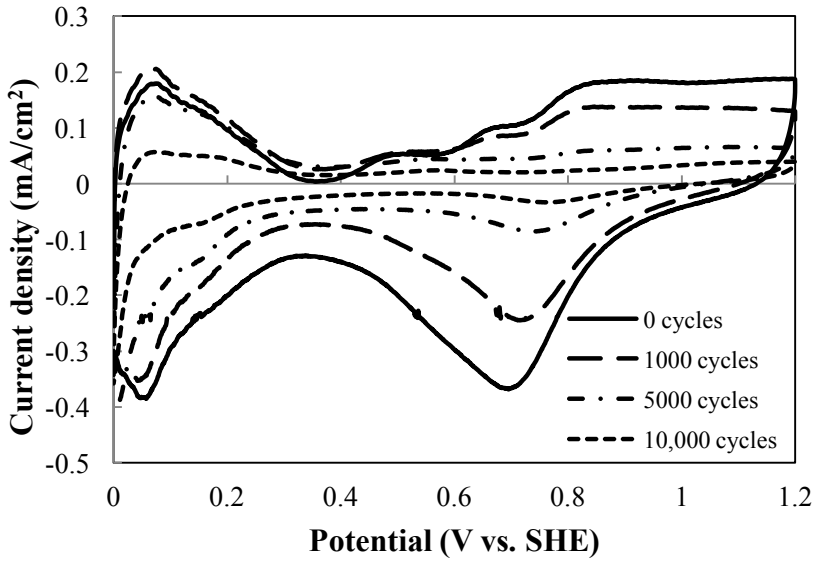

Figure 45. Cyclic voltammograms (at 20mV/s) of 40%Pt/ITO (formaldehyde reduction method) after 0, 1000, 5000 and 10000 cycles (load cycling accelerated degradation protocol). RDE experiment was conducted at room temperature in nitrogen saturated 0.1M perchloric acid.

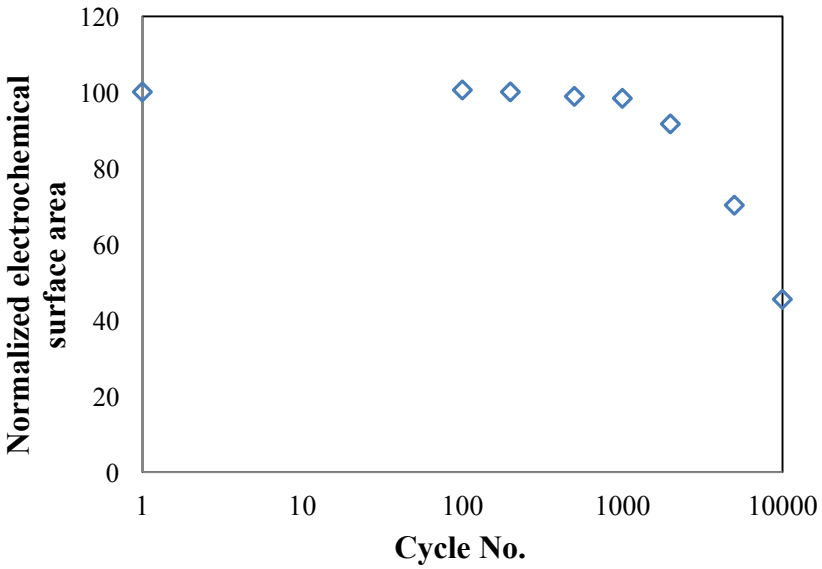

Figure 46. Normalized ECSA vs. cycle number for 40%Pt/ITO (formaldehyde reduction method) during load cycling accelerated degradation protocol.

We observed (from the data shown in **Figures 43-46** that the 40%Pt/ITO catalyst synthesized by reduction of $H_2PtCl_6 \cdot 6H_2O$ (onto ITO) with formaldehyde was very stable under start-up/shutdown accelerated degradation protocol. The ECSA change was less than 4% over 10,000 cycles. This is somewhat expected due to the passivation of the Pt particles at high potential, but this result also augured well for the exceptional stability of the support.

The load cycling accelerated degradation protocol (from 0.6 to 0.95 V vs. SHE), targeted towards catalyst dissolution, revealed high stability for a very respectable 1000 cycles. However, a decrease in ECSA of approximately 55% was observed after 10,000 cycles. A decrease in double layer capacitance was also observed. This indicated that Pt not only agglomerated, but was also lost during the test in the 0.1M perchloric acid. Further efforts are underway to enhance the stability of the Pt/ITO under load cycling by attempting to exploit metal support interactions.

4.5. PEMFC Polarization Curves with Pt/ITO Electrocatalyst

This past quarter, the focus of the work at NTCNA was on MEA testing of a large batch of Pt/ITO catalyst that has been tested and screened at the RDE level (results shown in Figure N3). The ink formulation that was used was the same as for the Pt/RTO sample in order to make a direct comparison with the MEA results of Pt/RTO (an ionomer:support mass ratio of 0.9 was used). The Pt/ITO ink was successfully sprayed onto SGL 25 BCH GDLs, and four 25 cm^2 MEAs were made using established protocols at Nissan.

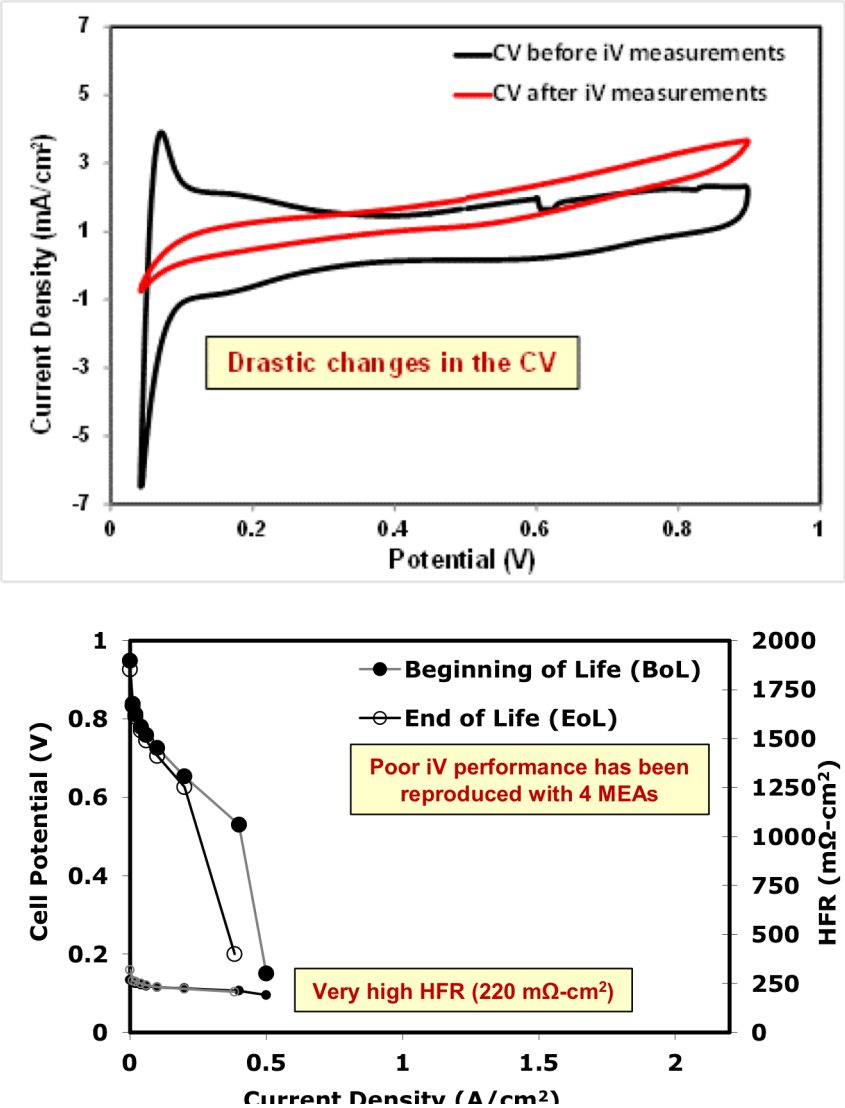

Figure 47. MEA Testing of Pt/ITO showing poor MEA performance of the catalyst. Cell conditions: H_2/O_2, 80°C, 100% RH, 1 bar_g backpressure. The poor MEA performance of Pt/ITO has been reproduced four times. Top: MEA cyclic voltammogram, bottom: MEA iV curve.

The MEA results for Pt/ITO are presented in **Figure 47**. The catalyst showed poor MEA performance even at a Pt loading of 0.35 mg/cm^2. The high frequency resistance (HFR) was observed to be very high (220 mΩ-cm^2, normally at ~60 mΩ-cm^2), suggesting some possible conductivity problems with the ITO support. Furthermore, as can be seen from the top figure, drastic changes in the CV profile (loss of H_{upd} features and *resistive* behavior) was observed, suggesting some changes in the chemical properties of the ITO support. It is possible that hydroxylated species may have formed on the ITO surface at fuel cell operating conditions during the iV curve measurements. Hydroxide and oxy-hydroxide species can form on the surface of ITO due to (1) hydrolysis and (2) incomplete

hydrolysis reactions. The solubility of these hydroxylated species ($In(OH)_3$, etc.) is quite low, so they could remain adsorbed on the ITO surface forming a passivating layer. This may explain the increase in ohmic resistance observed during MEA operation. The poor MEA performance of Pt/ITO has been reproduced with 4 MEAs.

Start-stop cycling durability test was also performed in order to determine changes in the beginning of life (BoL) and end of life (EoL) performance of Pt/ITO, and the results are shown in Figure N4 (bottom). The EoL performance does not appear to be significantly different than the BoL curve, indicating that the ITO support may be able to maintain its properties at its BoL state through 1,000 potential cycles from 1.0-1.5V during the start-stop cycling.

4.6. XPS of Pt Supported on ITO to Investigate Degradation Mechanism

To analyze any changes in the composition of the catalysts, the raw XPS spectra were fitted using XPSPeak software. The shift of In $3d_{5/2}$ and In $3d_{3/2}$ peaks towards higher binding energies can be seen as a consequence of the formation of hydroxides or oxy-hydroxides, and can be used to extract conclusions about the stability of the support during fuel cell operation. The introduction of hydroxide makes the In $3d_{5/2}$ peak shift to ~ 446 eV. The fitting functions were the peaks that describe the presence of the different species: oxide, hydroxide and oxyhydroxide. The relative peak areas represent the surface concentration of each species. The detailed information for 40%Pt/ITO catalyst before fuel cell operation is shown in **Figure 48**. Peak 1 (445 eV) was assigned to In^{3+} in the oxide **phase** (ITO); peak 2 (446 eV) was assigned to In^{3+} adjacent to hydroxides. Fitting results showed clearly that before fuel cell operation, In^{3+} was all in the oxide form in the catalyst.

After fuel cell operation for approx. 2 hours, the anode catalyst (40%Pt/ITO) was recovered and XPS performed. The data was fitted as described in the previous paragraph. **Figure 51** shows the XPS fitting results for 40%Pt/ITO at the anode, after fuel cell operation (In $3d_{5/2}$). Fitting results showed the presence of a peak at ~446 eV, initially assigned to In^{3+} adjacent to hydroxides. According with this fitting, hydroxide on the surface of ITO accounts for 4% of the total amount of In.

The same calculation and analyses were done using 40%Pt/ITO as cathode catalyst. Fitting results are shown in **Figure 50.** XPS (In $3d_{5/2}$) showed formation of hydroxide on the surface of ITO after fuel cell operation for the catalyst being used in the cathode. The surface hydroxide concentration was approx. 7%.

The surface lattice of ITO has rectangular spaces, one atomic layer deep (0.8 and 4.9 Å width and length approximately). We believe that oxygen loss from the borders create defects on the surface, and sites for hydrolysis and/or addition of hydroxide. The surface hydroxide is derived from hydroxylation of the disrupted ITO lattice and incomplete hydrolysis of the oxides on ITO surface. The presence of surface hydroxides increases the electrode resistivity affecting fuel cell performance.

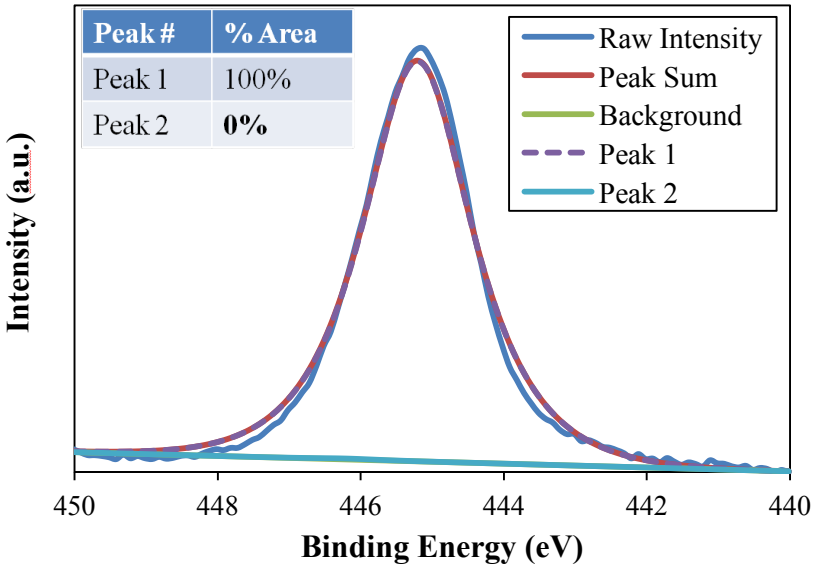

Figure 48. XPS fitting results for In $3d_{5/2}$ before fuel cell performance test. Peak 1 (445 eV) was assigned to In^{3+} in the oxide (ITO); Peak 2 (446 eV) was assigned to In^{3+} adjacent to hydroxides

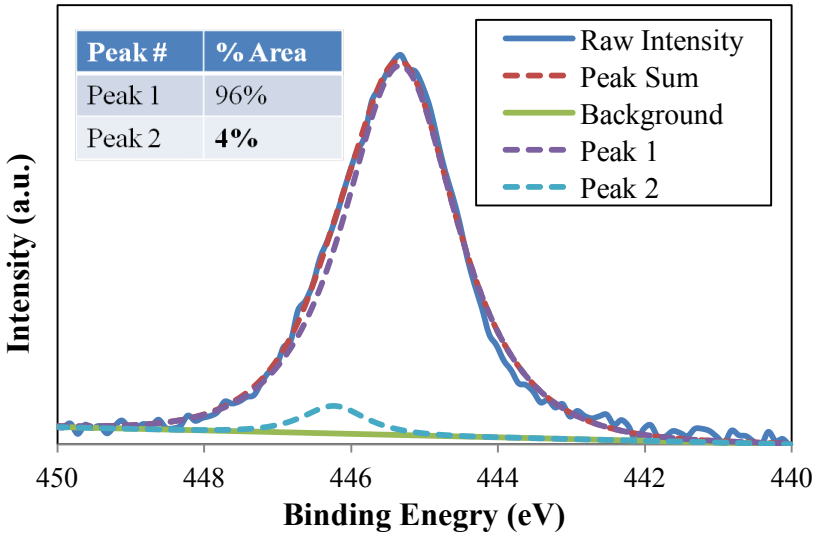

Figure 49. XPS fitting results for In $3d_{5/2}$ after fuel cell performance test in the anode. Peak 1 (445 eV) was assigned to In^{3+} in the oxide (ITO); Peak 2 (446 eV) was assigned to In^{3+} adjacent to hydroxides

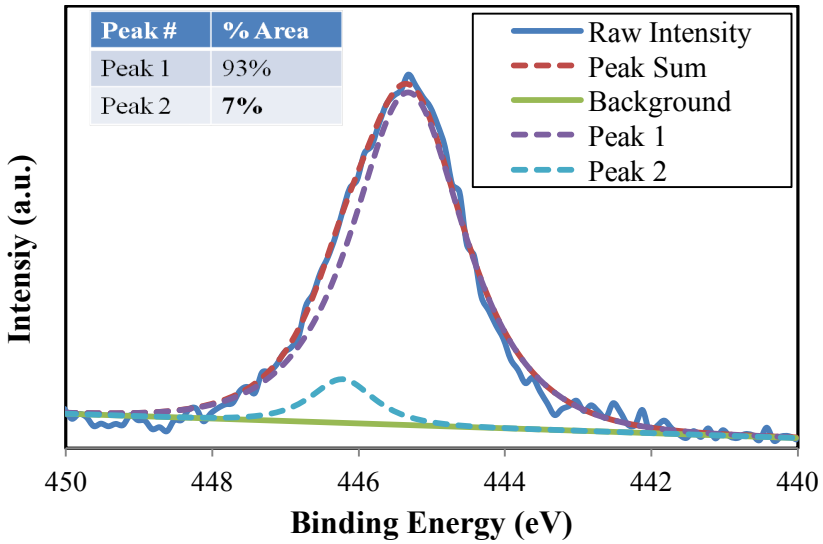

Figure 50. XPS fitting results for $In3d_{5/2}$ after fuel cell performance test in the cathode. Peak 1 (445 eV) was assigned to In^{3+} in the oxide (ITO); Peak 2 (446 eV) was assigned to In^{3+} adjacent to hydroxides

Figures 51-53 showed the XPS fitting results for O1s spectrum for 40%Pt/ITO before and after being employed as catalyst in the fuel cell. Peak 1 (530 eV) was assigned to ITO-like oxygen (oxides). Peak 2 (531 eV) was assigned to oxide that is adjacent to an oxygen deficiency site (oxygen vacancy); oxygen atoms adjacent to oxygen vacancies donate some of their electron density and hence shift slightly towards higher binding energies. Peak 3 (532 eV) was assigned to oxygen in the form of hydroxides. And finally, peak 4 was included to account for impurities (O-like) and improve the overall fitting. We found that the initial ITO contained only oxides (we did not find hydroxides). After the catalyst was used in the fuel cell (at either anode or cathode), we observed the formation of surface hydroxides (12 to 16%).

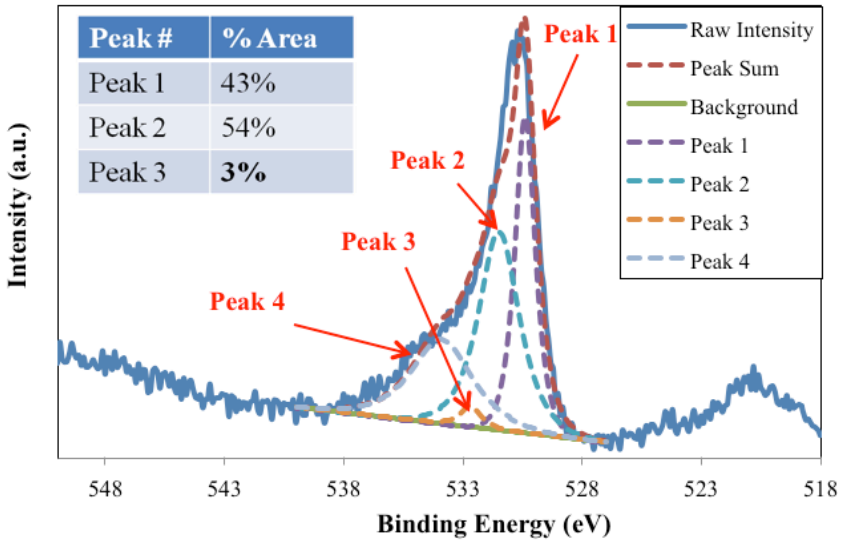

Figure 51. XPS fitting results for O 1s before catalyst used in the fuel cell. Peak 1 (530 eV) was assigned to oxides in the ITO. Peak 2 (531 eV) was assigned to oxide atoms adjacent to oxygen vacancies. Peak 3 (532 eV) was assigned to oxygen in the form of hydroxides. And peak 4 (accounting for impurities) was included to improve the overall fitting.

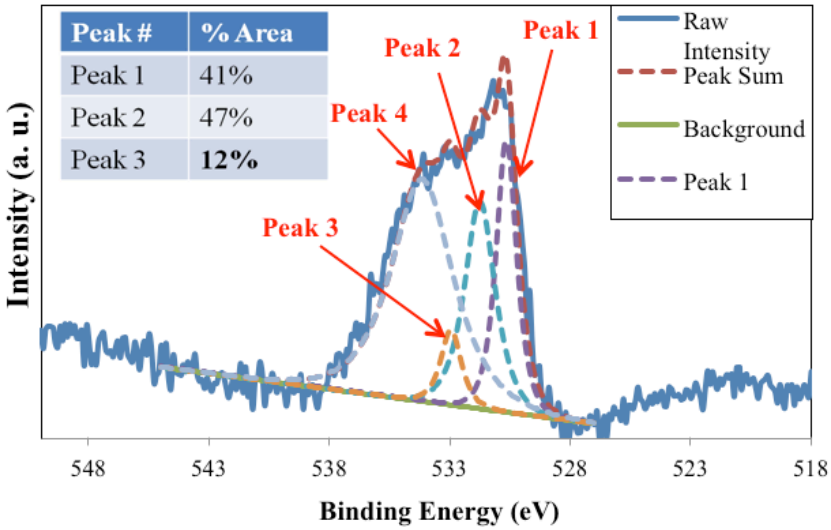

Figure 52. XPS results for O 1s after Pt/ITO used as anode catalyst in the fuel cell. Peak 1 (530 eV) was assigned to oxides in the ITO. Peak 2 (531 eV) was assigned to oxide atoms adjacent to oxygen vacancies. Peak 3 (532 eV) was assigned to oxygen in the form of hydroxide. And Peak 4 accounted for the presence of impurities.

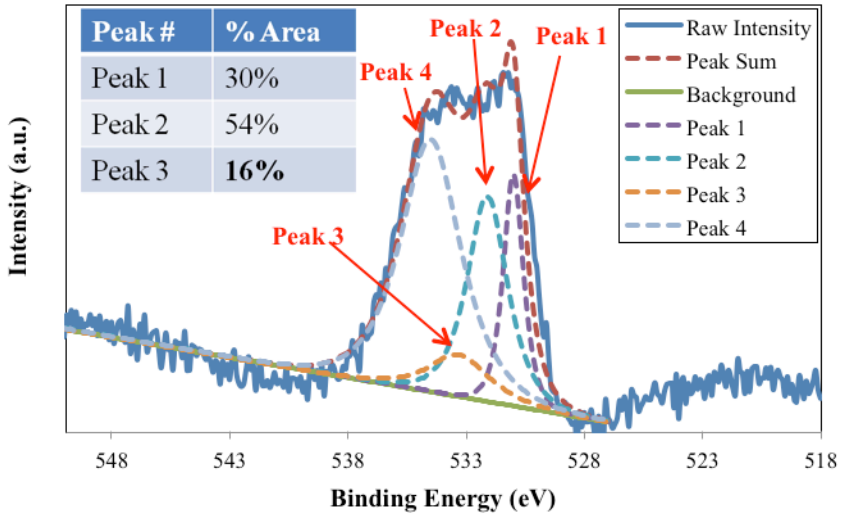

Figure 53. XPS results for O 1s after Pt/ITO being used as cathode in a fuel cell. Peak 1 (530 eV) was assigned to oxides in the ITO. Peak 2 (531 eV) was assigned to oxide atoms adjacent to oxygen vacancies. Peak 3 (532 eV) was assigned to oxygen in the form of

5. Indium Oxide Doped with Zirconium Oxide Catalyst Support

5.1. Synthesis of In_2O_3 Doped with ZrO_2

10 mol % of $ZrOCl_2 \cdot 8H_2O$ and 90 mol % of $InCl_3$ were dissolved in 20 ml of DI water. After stirring for 30 mins, 30 wt% ammonia solution was added dropwise under stirring to adjust the pH to 7 – 8. The precipitate was aged for 48 hours at 60 °C at room temperature. The precipitate was collected by filtration and washed by DI water and ethanol three times. The product was dried in an oven at 70 °C for 24 hours, and finally grounded into fine particles using a mortar and pestle. Pure In_2O_3 also was synthesized using same procedure. The material was finally annealed at 800 °C in air for 3 h.

5.2. Characterization of Indium Oxide Doped with Zirconium

XRD was used to confirm the doping effect of zirconia on the support and to obtain a quantitative estimate of their crystallite size. The main diffraction peaks were at 21.7°, 30.8°, 35.7°, 51.3° and 61° and corresponded to the diffractions of (211), (222), (400), (440) and (622) planes (See **Figure 54**) illustrates the shifting of one of the diffraction peaks as consequence of the doping. Pure In_2O_3 annealed at 800 °C has cubic phase. Zr-doped In_2O_3 by co-precipitation (90 mol % of In_2O_3,) and silica-template method showed the presence of cubic phase as in the case of In_2O_3. The presence of 10 mol % ZrO_2 caused the main diffraction peaks of Zr-doped In_2O_3 (10 mol: 90 mol = ZrO_2: In_2O_3) to shift towards low angles (or all (211), (222), (400), (440) and (622) atomic planes).

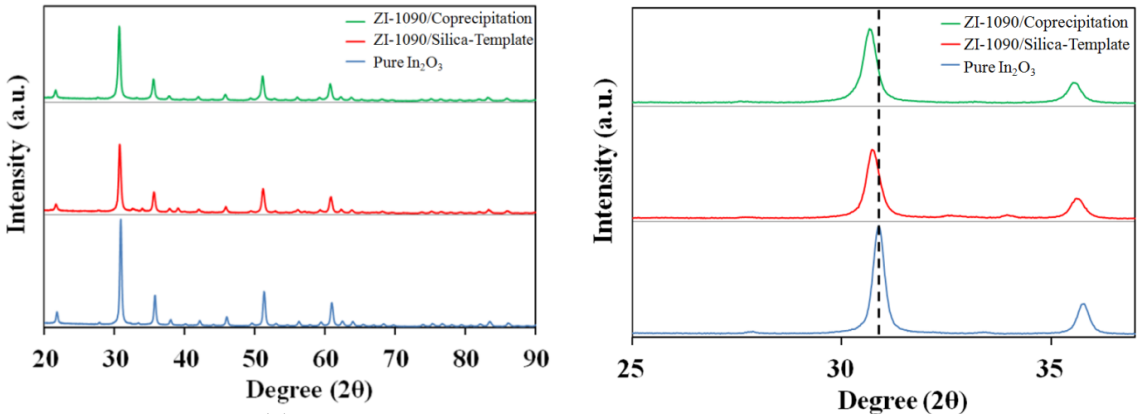

Figure 54. X-ray diffraction patterns of Zr-doped In_2O_3 (ZrO_2:In_2O_3 = 1:9 mol), annealed at 800 °C in air for 3 hours. (a) XRD patterns, (b) zoomed view of Fig 9a to show the shifting of peak (222).

5.3. Electrochemical Stability of ZrO_2-doped In_2O_3 Catalyst Support.

Stability of ZrO_2-doped In_2O_3 supports were characterized by performing potential cycling tests on a glassy carbon (GC) disk electrode in N_2 saturated 0.1M $HClO_4$ solution using a rotating disk electrode (RDE) setup. To make catalyst support ink, 4 mg of In_2O_3 doped with ZrO_2 was dissolved in 0.1 mL of DI water and 0.7 mL of isopropanol, followed by the addition of 25.9 µl Nafion® solution (5 wt %). After then, mixed solution was sonificated for 1 hour in ice water. 5 µL of the ink was then placed on the GC disk using 10µL micropipette and dried under ambient conditions. The final catalyst support loading on GC disk was controlled approximately to 120µg/cm^2_{disk}. In the RDE setup, a saturated calomel electrode was used as reference electrode and Pt foil was used as counter electrode. The supports were cycled between 1.0 to 1.5 V vs. (start-stop protocol) RHE at a scan rate of 500 mV/s for up to 10,000 cycles and cyclic voltammograms were recorded between 0.0 to 1.2 vs. RHE at periodic intervals at a scan rate of 20 mV/s. The stability of non-carbon support under start/stop operation was estimated by calculating the capacitances using three different methods (C_{dl}, C_{avg} and C_{int}). Details of how to calculate the capacitance are provided in following paragraphs. **Figure 55** shows the cyclic voltammograms employed to calculate the pseudo-capacitance.

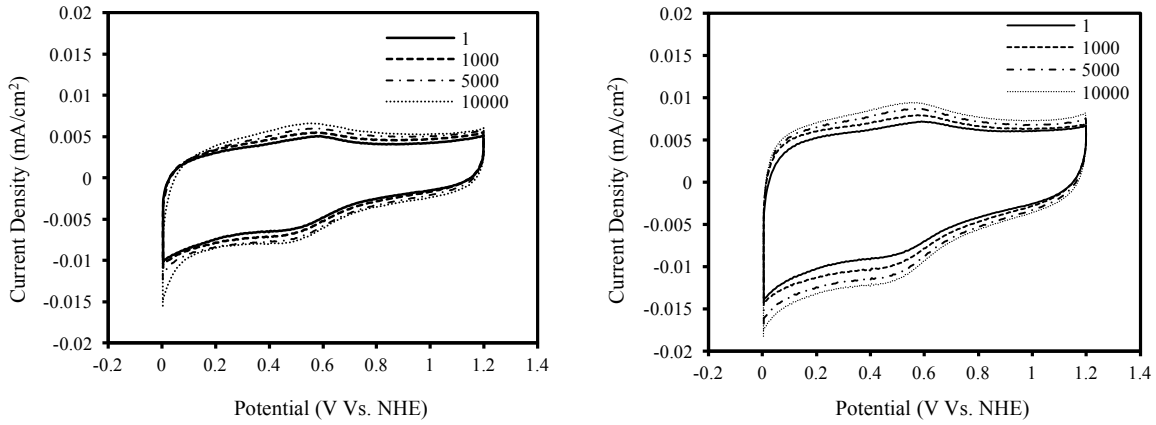

Figure 55. Cyclic voltammograms (CV) of Zr-doped In_2O_3 (ZrO_2:In_2O_3 = 1 mol: 9 mol) during start-stop stability experiment. (a) ZI-1090/Coprecipitation and (b) ZI-1090/Silica-Template.

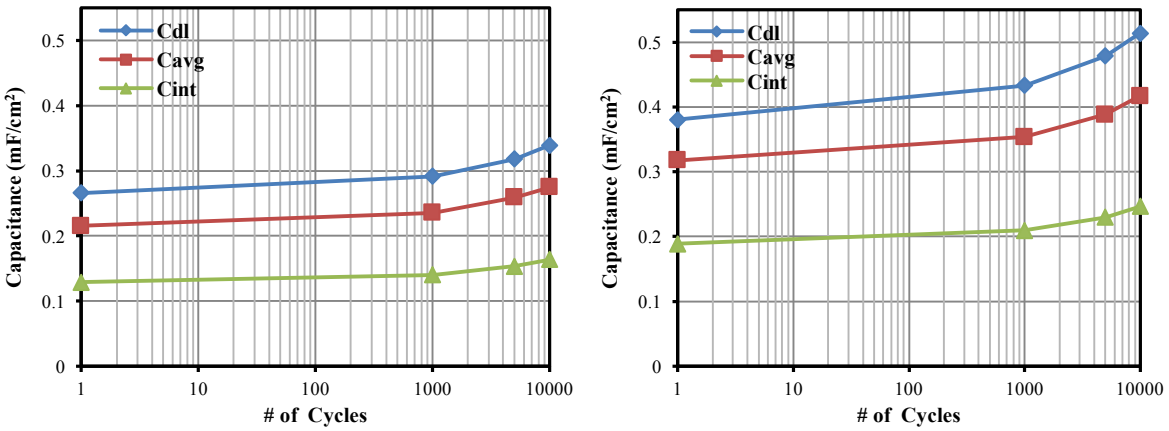

Figure 56. Change of catalyst support capacitance (calculated using three methods) during the potential cycling (start-stop protocol). (a) ZI-1090/copecipitation; (b) ZI-1090/silica-template.

C_{dl} (mF/cm^2) was calculated by dividing the current density at 0.4V_{SHE} (i_{dl}) by the scan rate (0.02 V/s). C_{avg} was calculated using an average current density (in the potential range from 0.1 V to 1.1V_{SHE}). C_{int} was calculated dividing the double layer charge, calculated integration of the CV curve in the potential range 0.1 to 1.1 V, by the potential difference (1 V). All the calculated capacitances also contain pseudo-capacitance. Due to the asymmetry in the CV curve, C_{int} is more adequate to evaluate the support stability. However, C_{dl} was also estimated to compare with previous data on other supports such as RuO_2-SiO_2, TiO_2-RuO_2 and ITO.

Figure 56 illustrates the change of the capacitance of ZI-1090/coprecipitation and ZI-1090/silica-template during potential cycling (start-stop protocol). Initially, ZI-1090/silica-template had a capacitance of 0.189 mF/cm^2 (C_{int}), which is higher than for ZI-1090/coprecipitation (0.129 mF/cm^2). Due to the different current density values used in the calculation, C_{dl}, C_{avg} and C_{int} had different values, but they all show the same trends. Figure 12 shows the normalized capacitances for indium oxide doped with zirconium. Capacitance changed 127% after 10,000 cycles for ZI-1090/coprecipitation, and 131 % for ZI -1090/silica-template. The two different synthesis methods result in materials with similar electrochemical stability as expected. **Table 5** shows the BET surface area for ZI-1090/silica-template (18.14 m^2/g , 800 °C), and ZI-1090/co-precipitation (16.64 m^2/g).

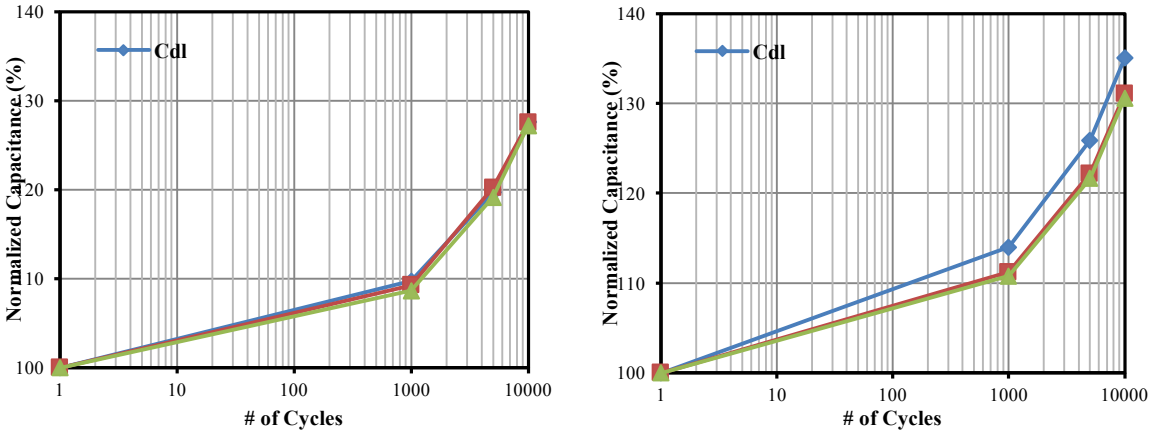

Figure 57. Normalized capacitances for (a) ZI-1090/co-precipitation (b) ZI-1090/silica-template

Table 5. BET surface area and electronic conductivity for zirconium doped indium oxide.

	Annealing Temperature		Electrical Conductivity	
Material	400 °C [m^2/g]	800 °C [m^2/g]	400 °C [S/cm]	800 °C [S/cm]
ZI-1090/coprecipitation	36.79	16.64	0.068 ± 0.002	0.086 ± 0.002
ZI-1090/silica-template	37.55	18.14	N/A	N/A

ZI-1090/coprecipitation (800 °C) had an electrical conductivity 0.086 S/cm. The doping with zirconium helped to increase the conductivity. The conductivity of pure ZrO_2 was only $1 \sim 2 \cdot 10^{-6}$ S/cm. We are currently optimizing the amount of zirconium needed to get an electrical conductivity close to 0.1 S/cm.

6. Cost Model for 40%Pt/RuO_2-TiO_2

40 wt% Pt/RuO_2-TiO_2 had shown excellent support durability under Nissan start-stop stability protocol in both RDE and MEA, as reported previously. The performance of the catalyzed sample in an MEA was also very comparable to baseline 50% Pt on Ketjen Black support catalyst. The biggest criticism for metal oxide based supports is the cost of the material compared to conventional carbon support, which is very inexpensive. The metal oxide based non-carbon supports may not be very cost competitive to carbon support when only material cost is considered, but owing to their excellent durability under automotive start-stop and load cycling accelerated tests, cost analysis of these non-carbon support has indeed become very essential. NTCNA has prepared a preliminary cost model for these non-carbon support materials considering their durability benefits. Material costs for production of Pt/ RuO_2-TiO_2 electrodes are compared to Pt/Vulcan XC-72. Data for Pt/Vulcan XC-72 used here is from 2008 FC cost system estimation from DOE. Assumptions made to simplify this model are a) except for the cathode rest of the MEA is identical; b) rated power is at 80°C, 100% RH; c) all the stacks in the cell are operating identical; d) processing costs (ink manufacturing, catalyst application etc..) are equal. Material costs of the cathodes are compared as shown in **Figure 58**.

As mentioned earlier, the biggest concern for metal oxide supports is that their cost is significantly more than carbon. As shown in **Table 6**, RuO_2-TiO_2 support is more expensive, but the total material cost is still dominated by platinum cost. Though ruthenium is considered a precious metal, its cost ($80-90/troy oz.) is far less than that of platinum ($1100/troy oz. – DOE standard). It should also be noted that ruthenium only makes up 38% of the mass of the support, while the rest is relatively inexpensive TiO_2.

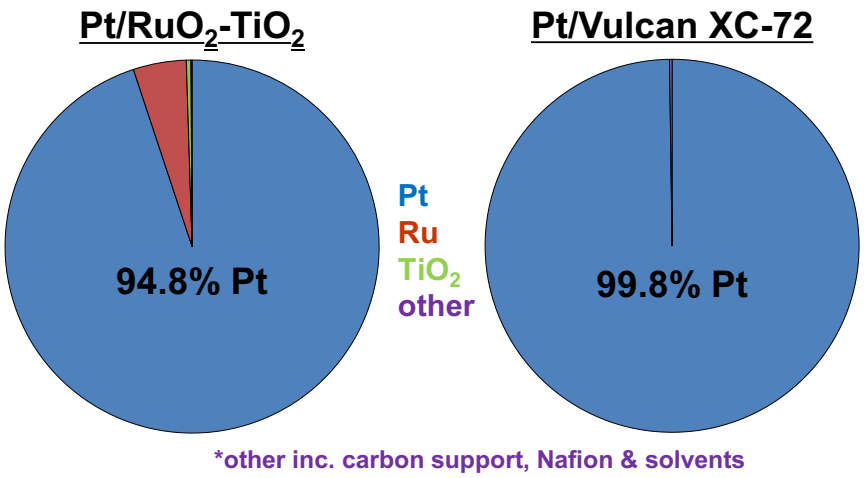

Figure 58. Cathode material cost comparison between Pt/non-carbon and Pt/Vulcan XC-72

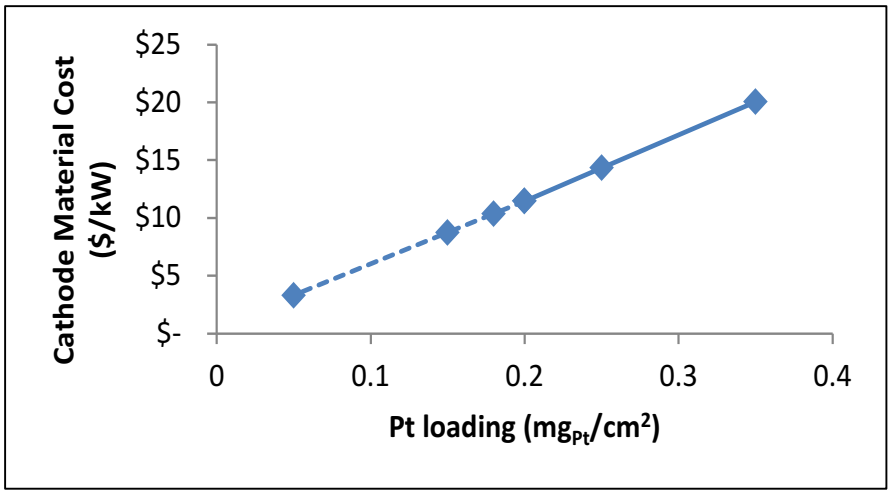

Figure 59. Potential cost reduction of cathode material by reducing Pt loading

As shown in **Figure 59**, significant cost reduction can be achieved by reducing the cathode Pt loading. Cathode material cost is virtually proportional to Pt loading.
The major advantage of using metal oxide support at the cathode is its excellent resistance to degradation under start-stop cycling. This durability needs to be considered while doing the cost analysis. Based on the data obtained for these two cathode materials; Pt/RTO and Pt/Vulcan XC-72 under the Nissan start-stop durability cycling, a so called "durability factor" was calculated using following equation:

$$\text{Durability Factor} = \frac{\text{Mass Activity retention of Catalyst}}{\text{Mass Activity retention of Pt/RuO}_2\text{–TiO}_2} \qquad [13]$$

Mass activity retention was chosen as a basis because the DOE target for catalyst support durability is defined in terms of mass activity. Pt/RTO retained 86% of its mass activity while Pt/Vulcan XC-72 retained only 66% of its initial mass activity under Nissan start-stop durability cycling. Based on this protocol, Pt/Vulcan XC-72 is only 69% as durable as the Pt/RTO. After considering the durability advantages of Pt/RTO, preliminary cost model shows that even with almost double the Pt loading (0.35 vs 0.18 mg$_{Pt}$/cm^2); Pt/RTO is only slightly more expensive than Pt/Vulcan XC-72 as shown in **Table 6**.

Table 6. Estimated cost of the materials for Pt/RuO_2-TiO_2, Pt/ITO and Pt/Vulcan XC-72.

	Pt/RuO_2-TiO_2	Pt/ITO	Pt/Vulcan XC-72
Cathode Pt loading (mg_{Pt}/cm^2)	**0.35**	**0.35**	**0.18**
Rated Power (mW/cm^2)	650	650*	715
Pt	$1,718.45	$1,718.45	$1,203.42
Metal 1	$90.31 (Ru=$83.02)	$34.68 (In=$34.61)	$ -
other	$3.00 (est.)	$3.00 (est.)	$2.64
Total Material Cost ($)	$1,811.76	$1756.14	$1,206.06
Total Material Cost ($/$kW_{net}$)	$22.65	$21.95	$15.08
Durability Factor	1	1	0.69
Total Material Cost ($/$kW_{net}$) w/ durability	**$22.65**	**$21.95**	**$21.85**

6.1. Comparison of Cost Models of 40%Pt/RuO_2-TiO_2 and 40%Pt/ITO

The material costs of the cathodes are compared in **Figure 60** and **Table 6** . As shown in the figure, the RTO support was more expensive than ITO and Vulcan, but the total material costs were still dominated by platinum cost. Although ruthenium is considered a precious metal, its cost ($80-90/troy oz.) is far less than that of platinum ($1100/troy oz. – DOE standard). It should also be noted that ruthenium only makes up 38% of the mass of the support, while the rest is relatively inexpensive TiO_2. This proportion can be further lowered. Furthermore, significant cost reduction can be achieved by reducing the cathode Pt loadings (cathode material costs were proportional to Pt loading).

Mass activity retention was chosen as a basis because the DOE target for catalyst support durability is defined in terms of mass activity. Pt/RTO retained 86% of its mass activity while Pt/Vulcan XC-72 retained only 66% of its initial mass activity under Nissan start-stop durability cycling. Based on this protocol, Pt/Vulcan XC-72 is only 69% as

durable as the Pt/RTO. After considering the durability advantages of Pt/RTO and assuming similar durability for Pt/ITO (justified thus far based on durability studies in the RDE), the preliminary cost model shows that even with almost double the Pt loading (0.35 vs 0.18 mgPt/cm^2); Pt/RTO and Pt/ITO are only 4% and 0.5% more expensive than Pt/Vulcan XC-72.

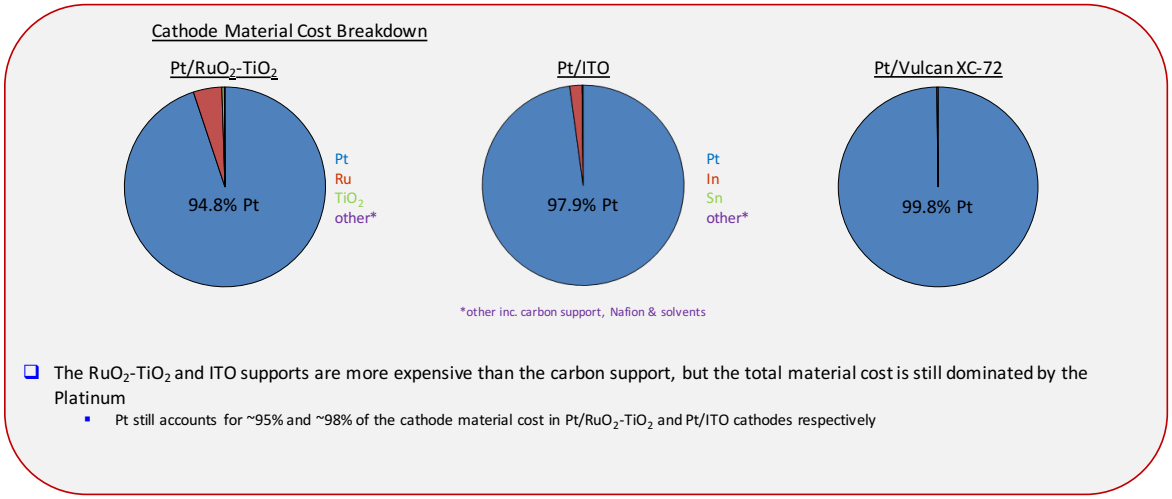

Figure 60. Cathode material cost comparison between Pt/RTO, Pt/ITO and Pt/Vulcan XC-72

7. Conclusions

An extensive search and evaluation of electrochemically stable catalyst supports was perfomed during the 4 years of the project. The suports were also catalyzed by deposition of Pt and tested for its performance and electrochemical stability. For testing the electrochemical stability and fuel cell performance of the catalysts and supports, we have employed the same protocols in use at the Department of Energy and Nissan Technological Center North America. The use of such procedures allows a precise and reproducible estimation of the performance and stability of the materials and permits comparisons among laboratories and DOE funded projects.

We succesfully synthesized RuO_2-SiO_2 catalyst supports with the following desirable properties: high BET surface areas (260 m^2/g), excellent electrical conductivity (up to 24 S/cm), and excellent electrochemical stability. The results showed no loss in surface area for the RuO_2-SiO_2 catalyst supports (start-stop stability tests were performed by cycling electrode potential between 0 V to 1.8 V for 1000 cycles), while a 44% drop in surface area was observed in carbon supports tested as a baseline. Catalyzed support (40% Pt/RuO_2-SiO_2; 1:1 mole ratio) were tested in a PEFC, resulting in a current density of 750 mA/cm^2 at 0.6 Volts, and a maximum power density of 570 mW/cm^2. Measurements were conducted at 80 ºC with 75% relative humidity of the inlet gases (H_2/O_2); Pt loadings were 0.4 mg/cm^2 at the cathode and 0.2 mg/cm^2 at the anode. We have also synthesized

functionalized silica supports with several levels of sulfonic acid functionalization. These materials have demonstrated varying degrees of proton conductivity and electrochemical stability. In general, the functionalization decreased the electrochemical stability (as measured by potential cycling protocols).

RuO_2-TiO_2 (RTO) catalyst supports possessed the following properties: excellent electrical conductivity (~ 22 S/cm), excellent electrochemical stability, and comparable fuel cell performance with Pt/C baseline. Start-stop stability tests for stand alone supports and MEAs were performed by potential cycling of the cell between 1 V to 1.5 V vs RHE for 10,000 cycles; both tests performed at Illinois Institute of Technology (IIT) and Nissan Technical Center, North America (NTCNA) have confirmed support durability. *In-situ* accelerated degradation experiments at NTCNA have established that using the RTO supports (synthesized and catalyzed at IIT), the beginning of life performance was exactly equal to end of life performance (in an MEA that has been subjected to severe start-stop cycling). This result was in sharp contrast to baseline Pt/C catalyst that showed significant performance deterioration after accelerated stability tests. The Pt/TRO showed minimal loss in performance upon exposure to start-stop cycles. The loss in cell voltage at 1 A/cm^2 at 100% RH was almost 700 mV for Pt/C whereas it was only ca. 15 mV for Pt/TRO. 40% RH data (of inlet gases) revealed a similar trend in terms of stability – exceptional stability for Pt/TRO as opposed to very poor stability for Pt/HSAC. These observations were attributed to the much higher stability of the TRO support compared to Carbon.

The carbon dioxide concentration in the cathode exit stream during the accelerated degradation test with Pt/TRO (start-stop protocol) was extremely low (between 3 to 10 ppm of CO_2). In contrast, the CO_2 emission levels from a conventional Pt/C catalyst were around 200 ppm. This observation was a clear indicator that the main source of carbon being oxidized to carbon dioxide in an MEA was the carbon catalyst support, and not the gas diffusion layer (GDL) or the graphite flow fields.

NTCNA performed a detailed analysis of transport phenomena (reactants and products to/from the Pt active sites) in both commercial catalyst and Pt/RTO (in order to have a better understanding at the basic level). The proton resistance ($R_{ionomer}$) in Pt/C and Pt/RTO cathode catalyst layers were 150 and 12 mΩ-cm^2, respectively. Pt/RTO catalyst layer has about an order or magnitude lower proton transfer resistance than Pt/C catalyst layer. Since the ionomer/support ratio that was used in formulating the ink for both catalysts was the same (0.9), it is expected that the volumetric coverage of ionomer of both catalysts will be significantly different due to the disparity in the surface areas (Pt/C had ~ 800 m^2/g, while Pt/RTO had ~ 50 m^2/g). The differences in the ionomer volumetric coverage and the ionomer film thickness may explain the significantly higher proton conductivity in the Pt/RTO catalyst layer when compared to Pt/HSAC. It is therefore very important to optimize the ionomer loadings when synthesizing new catalyst supports (and never rely on values for carbon-based commercial catalysts)

Indium tin oxide (ITO) was also evaluated as a catalyst support for PEFCs. The surface area for the ITO (after annealing at 820 ºC) was higher than 70 m^2/g. RDE testing of both 20% and 40% Pt/ITO showed mass activities of ~150 $mA/_{mgPt}$, comparable to

Pt/RTO. Pt/ITO was also very stable under start-up/shutdown accelerated degradation protocol (RDE tests in perchloric acid). The ECSA change was less than 4% over 10,000 cycles. The load cycling accelerated protocol (from 0.6 to 0.95 V vs. RHE) resulted in a loss of approximately 34% of the initial ECSA after 10,000 cycles. However, fuel cell testing resulted in a very low performing catalyst. XPS spectroscopy was employed to investigate the changes in the catalysts occuring during fuel cell operation. It was observed a shift of In $3d_{5/2}$ and In $3d_{3/2}$ peaks towards higher binding energies. This can be explained by the formation of hydroxides or oxy-hydroxides in the surface of the catalyst. O1s spectrum for Pt/ITO catalyst after being operated in the fuel cell, also confirmed the formation of significant amounts of surface hydroxides (12 to 16%). The surface hydroxide was derived from hydroxylation of the disrupted ITO lattice and incomplete hydrolysis of the oxides on ITO surface. The oxygen loss from the borders created defects on the surface, and sites for hydrolysis and/or addition of hydroxide The presence of surface hydroxides in the catalyst increased the electrode resistivity affecting fuel cell performance.

Finally, NTCNA has elaborated a cost model for non-carbon support materials considering their durability benefits. Material costs for production of Pt/ RuO_2-TiO_2 electrodes were compared to Pt/C. RuO_2-TiO_2 support was more expensive than carbon but the total material cost is still dominated by platinum cost. Though ruthenium is considered a precious metal, its cost is far less than that of platinum. It should also be noted that ruthenium only makes up 38% of the mass of the support, while the rest is relatively inexpensive TiO_2. After considering the durability advantages of Pt/RTO, cost model showed that even with almost double the Pt loading (0.35 vs 0.18 mg_{Pt}/cm^2), Pt/RTO ($\$22.7/kW_{net}$) is only slightly more expensive than Pt/Vulcan XC-72 ($\$21.9/kW_{net}$).

8. References

Han, T., N. Dale, K. Adjemian, V. Nallathambi and S. Barton (2011) "Electrochemical oxidation of surface oxides to partially recover the performance of non-PGM catalyst under fuel cell operation." ECS Trans. **41**: 2289-2296.

Ignaszak, A., Ye, S., Gyenge, E. (2009) J. Phys. Chem. C, **113**: 298-307.

Landsman, D. A., Luczak, F. J., In Handbook of Fuel Cells Fundamentals, Technology, and Applications; Vielstich, W., Gasteiger, H. A., Lamm, A., Eds.; John Wiley and Sons Ltd.: West Sussex, England, 2003; Vol. 4.

Lefebvre, M.C., Martin, R.B., Pickup, P.G. (1999) Electrochemical and Solid-State Letters, **2**: 259-1261.

Lo, C.-P., Ramani, V. (2012) "SiO_2-RuO_2: A Stable Electrocatalyst Support". ACS Applied Materials and Interfaces **4**: 6109–6116.

Lo, C.-P., Wang, G., Kumar, A., Ramani, V. (2013) "TiO_2-RuO_2 electrocatalyst supports exhibit exceptional electrochemical stability". Applied Catalysis B: Environmental **140–141**: 133–140.

Makharia, R., Mathias, M.F., Baker, D.R. (2005) Journal of the Electrochemical Society, **152**: A970-A977.

Mashio, T., Ohma, A., Yamamoto, S., and Shinohara, K. (2007) ECS Transactions, **11**: 529-540.

Nonoyama, N., S. Okazaki, A. Z. Weber, Y. Ikogi and T. Yoshida (2011). "Analysis of Oxygen-Transport Diffusion Resistance in Proton-Exchange-Membrane Fuel Cells." Journal of The Electrochemical Society **158**: B416-B423.

Ohma, A., K. Shinohara, A. Iiyama, T. Yoshida and A. Daimaru (2006). "Membrane and Catalyst Performance Targets for Automotive Fuel Cells by FCCJ Membrane, Catalyst, MEA WG. ." ECS Transactions **41**: 775-784.

Parrondo, J., Han, T., Niangar, E., Wang, C., Dale, N., Adjemian, K., Ramani, V. (2014) "Pt supported on titanium-ruthenium oxide: A remarkably stable electrocatalyst for hydrogen fuel cell vehicles". Proceedings of the National Academy of Sciences, **111**: 45-50.

Ralph, T. R. and M. P. Hogarth (2002). "Catalysis for low temperature fuel cells. Part I: The cathode challenges." Platinum Met. Rev. **46**: 3-14

9. Acronyms

BET: Brunauer, Emmett and Teller
CV: cyclic voltammograms
ECSA: electrochemical surface area
EIS: Electrochemical Impedance Spectroscopy
GC: glassy carbon
HSO_3-: sulfonic acid group
IEC: ion exchange capacity
NTCNA: Nissan Technical Center, North America
ORR: oxygen reduction reaction
PEFC: polymer electrolyte fuel cell
POSS: polyhedral oligomeric silsesquioxanes
Q_{DL}: double-layer charge
RDE: rotating disk electrode
RH: relative humidity
RHE: reversible hydrogen electrode
XC-72R: the name of commercial carbon black powder
XRD: X-ray diffraction